NASA CONTRACTOR REPORT

NASA CR-2633

PROJECT FOG DROPS V

Task I: A Numerical Model of Advection Fog

Task II: Recommendations for Simplified Individual Zero-Gravity Cloud Physics Experiments

C. William Rogers, William J. Eadie, Ulrich Katz, and Warren C. Kocmond

Prepared by
CALSPAN CORPORATION
Buffalo, N.Y. 14221
for George C. Marshall Space Flight Center

NATIONAL AERONAUTICS AND SPACE ADMINISTRATION • WASHINGTON, D. C. • DECEMBER 1975

1. REPORT NO.	2. GOVERNMENT ACCESSION NO.	3. RECIPIENT'S CATALOG NO.
NASA CR-2633		

4. TITLE AND SUBTITLE: Project Fog Drops V — Task I: A Numerical Model of Advection Fog, Task II: Recommendations for Simplified Individual Zero-Gravity Cloud Physics Experiments

5. REPORT DATE: December 1975

6. PERFORMING ORGANIZATION CODE:

7. AUTHOR(S): C. William Rogers, William J. Eadie, Ulrich Katz, and Warren C. Kocmond

8. PERFORMING ORGANIZATION REPORT #: M156

9. PERFORMING ORGANIZATION NAME AND ADDRESS:
Calspan Corporation
Buffalo, New York 14221

10. WORK UNIT NO.:

11. CONTRACT OR GRANT NO.: NAS8-30776

12. SPONSORING AGENCY NAME AND ADDRESS:
National Aeronautics and Space Administration
Washington, D. C. 20546

13. TYPE OF REPORT & PERIOD COVERED: Contractor Report

14. SPONSORING AGENCY CODE:

15. SUPPLEMENTARY NOTES:

16. ABSTRACT

A two-dimensional numerical model was used to investigate the formation and development of advection fog over the ocean. The model predicts the evolution of potential temperature, horizontal wind, water vapor content, and liquid water content in a vertical cross section of the atmosphere as determined by vertical turbulent transfer and horizontal advection, as well as radiative cooling and drop sedimentation in fog. The model is designed to simulate the formation, development, or dissipation of advection fog in response to transfer of heat and moisture between the atmosphere and the surface as driven by advection over horizontal discontinuities in the surface temperature. Results from numerical simulations of advection fog formation and development are discussed with reference to observational studies of marine fog. Recommendations are presented for an additional numerical modeling investigation to resolve some discrepancies between the predictions of the model and observations of advection fog formation and development over the ocean.

A survey of candidate fog or cloud microphysics experiments which might be performed in the low gravity environment of a shuttle-type spacecraft is presented. Recommendations are given for experiments which are relatively simple in nature and relevant to fog modification problems.

17. KEY WORDS	18. DISTRIBUTION STATEMENT
	Category: 47 and 66

19. SECURITY CLASSIF. (of this report)	20. SECURITY CLASSIF. (of this page)	21. NO. OF PAGES	22. PRICE
Unclassified	Unclassified	79	$4.75

For sale by the National Technical Information Service, Springfield, Virginia 22161

ACKNOWLEDGMENTS

The authors of the numerical modeling study of advection fog are indebted to Mr. Roland J. Pilié and Mr. Eugene J. Mack for numerous helpful discussions of results from Calspan observational studies of marine fog. Special thanks are due Mrs. Joyce L. Terrano for her careful typing of this report.

TABLE OF CONTENTS

Section 1

INTRODUCTION

Calspan Corporation has conducted research on warm fog properties and fog modification concepts under sponsorship of the National Aeronautics and Space Administration since 1963. Results of previous investigations, which have included theoretical and experimental studies of warm fog modification concepts, numerical simulations of fog seeding experiments, numerical modeling studies of radiation and advection fog, and fog life cycle studies have been documented in numerous NASA contractor reports (see e.g., NASA reports, CR-72, CR-368, CR-675, CR-1071, CR-1731, SP-212, CR-2078, CR-2079, and CR-2201). These investigations have played an important part in our understanding of fog and the complex meteorological processes that are involved in its formation, persistence, and dissipation. This report describes the results of the most recent investigation under Contract No. NAS8-30776 with George C. Marshall Space Flight Center.

Contract performance was under the technical cognizance of Mr. O.H. Vaughan, Jr., Aerospace Environment Division, Space Science Laboratory of the NASA Marshall Space Flight Center, Huntsville, Alabama. Mr. John Enders, Chief of the Aviation Safety Technology Branch, NASA Office of Aeronautics and Space Technology, provided encouragement and the necessary support for the accomplishment of this work.

Field experiments to test the concept of modifying warm fogs by seeding with sized hygroscopic materials and observational studies on both radiation and advection fog have shown that a thorough understanding of complex natural processes of fog formation, development, and dissipation is required to effectively design and implement fog modification techniques. Working toward this end, a one-dimensional numerical model of radiation fog was developed and tested against comprehensive field observations of valley fog (Pilie et al., 1972). To further extend understanding of the processes

which determine the life cycles of fogs, a preliminary two-dimensional numerical model of advection fog was developed by Calspan (Mack et al., 1972) under joint sponsorship of NASA and the Naval Air Systems Command. While the usefulness and basic capabilities of the advection fog model were demonstrated, considerable potential for important research with the model remained.

In this investigation, the capabilities of advection fog model were further developed and delineated. The model was improved by including prognostic equations for the horizontal wind and by incorporating the influences of both the predicted wind shear and temperature gradient upon the turbulent exchange coefficients. To establish the range of validity of the model and to delineate important areas for further development and application of the model, fog formation and development processes over an ocean surface were simulated using the advection fog model, and the results were compared with recent Calspan observational studies of sea fog (Mack et al., 1975). The physical and mathematical foundations of the advection fog model and the results of numerical experiments with the model are discussed in Section 2. Recommendations are presented for future modeling research which builds upon the improvement and testing of the advection fog model in the present study.

In addition, a survey was carried out of candidate fog or cloud physics experiments for the zero-G environment of a shuttle-type spacecraft. Emphasis was placed on defining experiments which are simple in nature and relevant to fog modification problems. The survey and recommendations for zero-G experiments are presented in Section 3.

Section 2

A NUMERICAL MODEL OF ADVECTION FOG

2.1 INTRODUCTION

The principal effort under this program was devoted to improving a preliminary two-dimensional numerical model of advection fog developed under NASA sponsorship (Mack et al., 1972) and to establishing the range of validity of the improved model. The primary improvements to the model were the incorporation of prognostic equations for the horizontal wind and the utilization of turbulent exchange coefficients which depend on both the predicted wind and potential temperature gradients near the surface. The improved model predicts the evolution of potential temperature, water vapor content, liquid water content, and the horizontal wind in a vertical plane as determined by the processes of vertical turbulent transfer and horizontal advection, as well as radiative cooling and drop sedimentation in fog. The model is designed to simulate the formation, development, or dissipation of advection fog in response to fluxes of heat and moisture to or from the atmosphere to the surface as driven by horizontal discontinuities in the surface temperature.

The improved advection fog model was applied to simulate fog formation and development over an ocean surface, where the boundary condition at the surface leads to the transfer of water vapor and heat to or from the model atmosphere in response to advection over surface temperature changes. Results obtained from numerical experiments with the advection fog model have been compared with results from the Calspan observational studies of fog at sea (Mack et al., 1975) to delineate the range of validity of the model and to suggest fruitful directions for future model improvements and applications.

The physical and mathematical foundations of the numerical model are presented in Section 2.2. Documentation of the computer program for the two-dimensional advection fog model is provided in Appendix A. In Section 2.3,

results of numerical experiments on the formation and development of advection fog are discussed. Recommendations are presented in Section 2.4 for future numerical modeling research which builds upon the advection fog model development and testing in the present study.

2.2 NUMERICAL MODEL

2.2.1 Major Assumptions

The following assumptions are adopted in the numerical modeling study of advection fog:

(a) The model is two-dimensional in the x-z plane. All of the quantities are uniform in the y direction.

(b) The model is a boundary layer model in which dynamic processes are neglected.

(c) Vertical turbulent transfer is parameterized in terms of turbulent exchange coefficients.

(d) In the absence of fog, radiative flux divergence is neglected.

(e) No microphysical calculations are carried out. All influences of the fog microphysics in the model are parameterized in terms of the predicted liquid water content.

(f) Supersaturated water vapor condenses instantaneously until saturation is achieved. Liquid water in an unsaturated region evaporates instantaneously until saturation is achieved or the liquid water is exhausted.

2.2.2 Equations

- List of Symbols

In order to avoid lengthy explanations in the text, a list of the most important symbols employed will be given first:

T,Θ	temperature and potential temperature of air
r	water vapor mixing ratio
r_s	saturation mixing ratio
w	liquid water mixing ratio
u	horizontal wind component in x direction
u_g	geostrophic wind
v	horizontal wind component in y direction
z	height coordinate
k	subscript denoting kth vertical grid level
x	horizontal coordinate
i	subscript denoting ith horizontal grid column
t	time
n	superscript denoting nth time step
K_m	turbulent exchange coefficient for vertical turbulent transfer of momentum
K_h	turbulent exchange coefficient for vertical turbulent transfer of heat and moisture
ρ	density of air
C_p	specific heat of air at constant pressure
R	net upward flux of infrared radiation
σ	Stefan-Boltzmann constant
P	air pressure
L	latent heat of condensation
V_t	mean terminal velocity of fog drops
k_w	spectrally-averaged mass absorption coefficient of fog for infrared radiation ($cm^2\ g^{-1}$)
g	gravitational constant

f	Coriolis parameter
u^*	friction velocity
H	heat flux in constant flux layer
L_s	$-U^{*3}C_p\rho T/kgH$ Monin-Obukhov scaling length
z_o	roughness height
k	von Karman constant = 0.4

- Major Equations

The equations employed in the model for the time rate change of potential temperature Θ, water vapor mixing ratio r, liquid water mixing ratio w, wind component u, and wind component v are:

$$\frac{\partial \Theta}{\partial t} = -u \frac{\partial \Theta}{\partial x} + \frac{\partial}{\partial z} \left(K_h \frac{\partial \Theta}{\partial z}\right) + \frac{1}{\rho C_p} \left(\frac{1000}{P}\right)^{2/7} \cdot \left(L \cdot C - \frac{\partial R}{\partial z}\right) \tag{1}$$

$$\frac{\partial r}{\partial t} = -u \frac{\partial r}{\partial x} + \frac{\partial}{\partial z} \left(K_h \frac{\partial r}{\partial z}\right) - C \tag{2}$$

$$\frac{\partial w}{\partial t} = -u \frac{\partial w}{\partial x} + \frac{\partial}{\partial z} \left(K_h \frac{\partial w}{\partial z}\right) + C + \frac{\partial}{\partial z} \left(V_t w\right) \tag{3}$$

$$\frac{\partial u}{\partial t} = -u \frac{\partial u}{\partial x} + \frac{\partial}{\partial z} \left(K_m \frac{\partial u}{\partial z}\right) + f \cdot v \tag{4}$$

$$\frac{\partial v}{\partial t} = -u \frac{\partial v}{\partial x} + \frac{\partial}{\partial z} \left(K_m \frac{\partial v}{\partial z}\right) + f \cdot (u_g - u) \tag{5}$$

- Saturation Adjustment

The symbol C denotes a source function for condensation or evaporation. In the actual model, the finite-difference approximations to Eqs. (1) through (5) are integrated for a time step, neglecting condensation or evaporation. Then, the saturation adjustment procedure developed by McDonald (1963)

is applied to the new values of Θ, r, and w. Taking into account the heating of the air by the release of latent heat of condensation, supersaturated water vapor at a grid point is converted into liquid water until saturation is achieved. Similarly, taking into account the cooling of the air, liquid water at a grid point is evaporated into an unsaturated vapor until saturation is achieved or the liquid water is exhausted.

- Turbulent Exchange Coefficients

As in earlier fog modeling studies (Pilié et al., 1972; Mack et al., 1972), the most difficult area in this advection fog modeling study was providing a realistic description of the vertical turbulent transfer of heat, moisture, and momentum over wide ranges of height and stability. In the present model, vertical turbulent transfer is parameterized in terms of flux-gradient relations using turbulent exchange coefficients. The turbulent exchange coefficients employed in the model are based on empirical flux-gradient relations which have been measured in studies of turbulent transfer in the lowest 50 m or so of the atmosphere (Businger et al., 1971; Panofsky, 1974), where the vertical fluxes of horizontal momentum and heat can be assumed constant with height, and the Coriolis force can be neglected. The extension of the flux-gradient relations obtained for steady-state, horizontal homogeneous atmospheric surface layers to the time varying, nonhomogeneous atmosphere boundary layers in the advection fog model imposes one of the prinicpal limitations to the realism of the model. Nevertheless, in absence of well-established higher order closure methods for the prediction of turbulent transfer under these conditions, the K-theory approach was adopted for this advection fog model to provide a simple, easily understood approximation to turbulent transfer of the type employed in earlier fog modeling studies.

By definition in the constant flux layer (Lumley and Panofsky, 1964), the turbulent exchange coefficient for momentum K_m is given by

$$u_*^2 = K_m \frac{\partial V}{\partial z} \tag{6}$$

where the friction velocity $u^* = \sqrt{\tau/\rho}$ is defined in terms of magnitude τ of the surface stress vector and $\frac{\partial V}{\partial z}$ is the magnitude of the horizontal wind shear. Similarly, the turbulent exchange coefficient for heat K_h is defined by

$$H = -\rho C_p K_h \frac{\partial \Theta}{\partial z} , \tag{7}$$

where H is the vertical heat flux, and $\frac{\partial \Theta}{\partial z}$ is the vertical gradient in potential temperature. Within the constant flux layer, it can be shown that the non-dimensional wind shear can be expressed in the form

$$\frac{kz}{u^*} \frac{\partial V}{\partial z} = \phi_m\left(\frac{z}{L_s}\right) , \tag{8}$$

where $L_s = -u^{*3} C_p \rho T/kgH$ is Monin-Obokhov scaling length. Similarly, the non-dimensional temperature gradient can be expressed in the form

$$\frac{z}{T^*} \frac{\partial \Theta}{\partial z} = \phi_h\left(\frac{z}{L_s}\right) , \tag{9}$$

where the scaling temperature is $T^* = -\frac{1}{ku^*} \frac{H}{\rho C_p}$.

By definition, then, within the constant flux layer, the exchange coefficient for momentum is

$$K_m = \frac{u^* kz}{\phi_m\left(\frac{z}{L_s}\right)} , \tag{10}$$

and exchange coefficient for heat is

$$K_h = \frac{u^* kz}{\phi_h\left(\frac{z}{L_s}\right)} \tag{11}$$

In the advection fog model, these turbulent exchange coefficients are multiplied by the factor exp[-8fz/u*], obtained by Shir (1973) in a numerical study of a neutral boundary layer, to provide for a reasonable behavior of the turbulent exchange coefficients at heights above the constant flux layer in the model.

In the model, non-dimensional wind shear $\phi_m(\frac{z}{L_s})$ and temperature gradient $\phi_h(\frac{z}{L_s})$ relations are employed which are based upon atmospheric measurements near the surface under relatively steady-state and horizontally homogeneous conditions (Panofsky, 1974). Under stable conditions or $L_s>0$, the relations

$$\phi_m = \phi_h = 1 + 5 \frac{z}{L_s} \tag{12}$$

are used. Under unstable conditions or $L_s<0$ relations

$$\phi_m = (1 - 15 \frac{z}{L_s})^{-\frac{1}{4}} \tag{13}$$

and

$$\phi_h = \phi_m^2 = (1 - 15 \frac{z}{L_s})^{-\frac{1}{2}} \tag{14}$$

are employed. Under neutral conditions or H = 0, both the stable and unstable relations reduce to

$$\phi_h = \phi_m = 1 \tag{15}$$

In applying the advection fog model to study fog formation at sea, the roughness height z_o was taken to be 0.01 cm in accordance with wind measurements at sea (Hsu, 1974). The first vertical grid level z_1 in the model was placed at 10 cm height. In order to calculate the friction velocity u*, the heat flux H, and the fluxes of momentum, and moisture between surface and first grid level, the non-dimensional gradient relations were integrated

between z_0 and z_1 under the assumption that buoyancy has no influence on the gradient relations at heights below 10 cm. Because the grid system of the model was aligned so that the geostrophic wind u_g is the x direction, the horizontal wind at the first vertical grid level z_1 has both an x and y component. Assuming that the horizontal wind components u and v are zero at the roughness height z_0, the following expression is used to compute the friction velocity

$$u^* = \sqrt{\tau/\rho} = \frac{k}{\ln(\frac{z_1}{z_0})} \sqrt{u(z_1)^2 + v(z_1)^2} \quad , \tag{16}$$

where $u(z_1)$ and $v(z_1)$ are the predicted horizontal wind components at the first grid level. Similarly, the stress components in the x and y directions are

$$\tau_x = \frac{k^2\rho}{[\ln(\frac{z_1}{z_0})]^2} \sqrt{u(z_1)^2 + v(z_1)^2} \cdot u(z_1) \tag{17}$$

and

$$\tau_y = \frac{k^2\rho}{[\ln(\frac{z_1}{z_0})]^2} \sqrt{u(z_1)^2 + v(z_1)^2} \cdot v(z_1) \tag{18}$$

Applying a similar reasoning to the potential temperature gradient between z_0 and z_1, the following expression is used to compute the heat flux between the surface and the first grid level

$$H = - \frac{k^2\rho C_p}{[\ln(\frac{z_1}{z_0})]^2} \sqrt{u(z_1)^2 + v(z_1)^2} \cdot (\Theta(z_1) - \Theta(z_0)) \tag{19}$$

where $\Theta(z_0)$ is taken to be the boundary value on potential temperature. Similarly, the flux of water vapor between the surface and the first grid level is computed from the expression

$$F_r = - \frac{k^2 \rho}{[\ln(\frac{z_1}{z_0})]^2} \sqrt{u(z_1)^2 + v(z_1)^2} \cdot (r(z_1) - r(z_0)) \tag{20}$$

where $r(z_0)$ is taken to be the boundary value on water vapor mixing ratio at the surface. The turbulent flux of liquid water between the surface and the first grid level is computed from the expression

$$F_w = - \frac{k^2 \rho}{[\ln(\frac{z_1}{z_0})]^2} \sqrt{u(z_1)^2 + v(z_1)^2} \cdot w(z_1) \tag{21}$$

where the boundary value on liquid water mixing ratio at the surface $w(z_0)$ is assumed to be zero.

In the integration of the advection fog model, the quantities u*, H, and L_s are evaluated for every grid column at the end of each time step. The turbulent exchange coefficients K_m and K_h are, then, computed for every grid point in the model from Eqs. (10) and (15), using the friction velocity u* and the scaling length L_s determined for the column. In accordance with the current practice (Panofsky, 1974), the turbulent exchange coefficients for the transfer of water vapor and liquid water are assumed equal to turbulent exchange coefficient for heat K_h. Because of the implicit integration procedure used to integrate the vertical transfer terms in the finite-difference equations of the model, the fluxes H, F_w, F_r, τ_x, and τ_y are converted into an effective turbulent exchange coefficient

$$K_m(\frac{z_1}{2}) = K_h(\frac{z_1}{2}) = \frac{k^2 \cdot z_1}{[\ln(\frac{z_1}{z_0})]^2} \sqrt{u(z_1)^2 + v(z_1)^2} \tag{22}$$

which is used in the finite-difference equations to compute the turbulent fluxes between surface and first vertical grid level z_1.

Making use of Eq. (6) to eliminate u*, and using the relation (Panofsky, 1974)

$$\frac{z}{L_s} = \phi_m\left(\frac{z}{L_s}\right) \frac{K_h}{K_m} Ri \tag{23}$$

to eliminate $\frac{z}{L_s}$, Eqs. (10) through (15) can be converted into expressions for turbulent exchange coefficients K_m and K_h in terms of the velocity gradient $\sqrt{\left(\frac{\partial u}{\partial z}\right)^2 + \left(\frac{\partial v}{\partial z}\right)^2}$ and the gradient Richardson number

$$Ri = \frac{\frac{g}{\Theta} \frac{\partial \Theta}{\partial z}}{\left(\frac{\partial u}{\partial z}\right)^2 + \left(\frac{\partial v}{\partial z}\right)^2} \tag{24}$$

Turbulent exchange coefficients of this type were initially utilized in this numerical modeling study of advection fog. A dependence of the turbulent exchange coefficients on the predicted local gradients of potential temperature and wind was believed to permit a more realistic description of the formation and development of advection fog than a dependence only on the predicted surface fluxes, even though both forms were derived from the same constant flux layer relationships. Unfortunately, computational instabilities were encountered in the integrations of the two-dimensional advection fog model with the turbulent exchange coefficients depending on the local wind shear and Richardson number, which could not be eliminated within the cost and time constraints of the program. Therefore, the dependence of the turbulent exchange coefficients on surface fluxes discussed above was adopted in the advection fog model to achieve computationally stable integrations.

- Radiation

The treatment of radiation in the present model is designed to capture the essence of physical processes while avoiding detailed radiative transfer calculations. In the absence of fog, the radiative flux divergence $\frac{\partial R}{\partial z}$ in Eq. (1) is assumed to be everywhere zero. In the presence of fog, a

radiative flux divergence representing the absorption and radiation of infrared radiation by fog drops is introduced into Eq. (1). An approximation expression relating the radiative flux divergence $\frac{\partial R}{\partial z}$ to the vertical distribution of the liquid water mixing ratio w(z) in the model is obtained by employing a spectrally-averaged mass absorption coefficient k_w to represent the influences of fog on radiative transfer. For simplicity, the fog is assumed to be at the absolute temperature T_o of the surface, thereby neglecting the influences of temperature gradients on the radiative transfer in the model fog.

It is assumed that a flux radiation equal to the black body radiation from the surface is transferred upward through the fog or

$$R_u(z) = \sigma T_o^4 \ . \tag{25}$$

Under clear sky conditions, it is also assumed that a downward flux of back radiation from the atmosphere equal to approximately 75% of the black body radiation from the surface is incident on the fog top at height z_T (Sutton, 1953) or

$$R_d(z_T) = .75\sigma T_o^4 \tag{26}$$

This downward flux of radiation on the fog top from the atmosphere is deficient in energy in the water vapor window portion of the spectrum between approximately 8.5 and 12 μm wavelength.

Inside the fog, the downward flux of radiation is determined by absorption and radiation of energy by the fog. At height z in the fog, the downward flux of radiation is

$$\begin{aligned} R_d(z) &= .75\sigma T_o^4 \exp\left[-1.6\int_z^{z_T} k_w(z')\rho w(z')dz'\right] \\ &\quad + \sigma T_o^4 \int_z^{z_T} 1.6\, k_w(\zeta)\, \rho w(\zeta) \exp\left[-1.6\int_z^{\zeta} k_w(z')\rho w(z')dz'\right]d\zeta \\ &= \sigma T_o^4 \left\{1 - .25\exp\left[-1.6\int_z^{z_T} k_w(z')\rho w(z')dz'\right]\right\} \end{aligned} \tag{27}$$

The first term on the right represents the downward flux of radiation incident on the fog top as attenuated through absorption by the fog in the distance from z_T to z. In the second term on the right, the downward radiation reaching height z due to radiation from an element of fog of thickness $d\zeta$ at height ζ is integrated from height z to the fog top at height z_T. Here the product $\rho w(z)$ of the density of air times the liquid water mixing ratio is the liquid water content of the model fog at height z. The influence of the angular dependence of the radiation field has been approximated by increasing the optical path lengths by the diffusivity factor 1.6 (Goody, 1964).

The net radiative flux at height z in the fog becomes

$$R(z) = R_u(z) - R_d(z) = .25\sigma T_o^4 \exp[-1.6\int_z^{z_T} k_w(z')\rho w(z')dz'] \qquad (28)$$

Differentiating with respect to z, we obtain the expression used in the model for the radiative flux divergence produced by fog

$$\frac{\partial R}{\partial z}(z) = .25\sigma T_o^4 1.6 k_w(z)\rho w(z)\exp[-1.6\int_z^{z_T} k_w(z')\rho w(z')dz'] \qquad (29)$$

To determine the form for the mass absorption coefficient k_w employed in the model, we must consider the absorption cross sections of fog drops. For fog drops of radius greater than approximately 4.5 μm, Zdunkowski and Nielsen (1969) have shown that the spectrally-averaged absorption cross section of a fog drop for black body radiation is within 20% of πr^2, where r is the radius of the drop. For a fog drop concentration of N drops per unit volume, the absorption per unit length in the model fog is assumed to be

$$1.6\ k_w \rho w = 1.6\ N\pi r^2 \qquad (30)$$

where r is the mean radius of the fog drops.

Solving for the mean fog drop radius r from the relation

$$N\rho_1 \frac{4\pi}{3} r^3 = \rho w \tag{31}$$

we obtain

$$r = \left(\frac{3\rho w}{4\pi\rho_1 N}\right)^{\frac{1}{3}} \tag{32}$$

Substituting for r in Eq. (30), we obtain the expression

$$1.6\ k_w \rho w = 1.6(\pi N)^{\frac{1}{3}} \left(\frac{3}{4\pi\rho_1}\right)^{\frac{2}{3}} (\rho w)^{\frac{2}{3}} \tag{33}$$

for the absorption per unit path length in the fog.

Assuming a constant drop concentration of N = 50 drops per cm^3, reasonably representative of coastal advection fogs (Mack et al., 1975), Eq. (33) reduces to expression

$$1.6\ k_w \rho w = 7.1(\rho w)^{\frac{2}{3}} cm^{-1} \tag{34}$$

for the absorption per cm employed in the fog model as a function of the predicted liquid water content ρw in grams per cm^3. To calculate the radiative flux divergence $\frac{\partial R}{\partial z}$ in the potential temperature equation of the model, the quantity $1.6\ k_w(z)\ w(z)$ in Eq. (29) is replaced by $7.1(\rho w(z))^{\frac{2}{3}}$, and the vertical integral is evaluated numerically. While this procedure is a crude approximation to radiative transfer in fogs (see Korb and Zdunkowski (1970) for detailed radiative transfer calculations in fog), it should provide a roughly quantitative simulation of the alteration of the vertical distribution of net radiation by fog and the accompanying radiative cooling of the fog. It has the advantage of imposing no significant computational requirements.

- Terminal Velocity of Fog Drops

In the model, the sedimentation of the fog drops is simulated through the mean terminal velocity V_t in Eq. (3). Under the assumption that the total drop concentration in the model fogs is constant, V_t is a function of the local liquid water mixing ratio which allows V_t to remain small until the predicted liquid water contents approach values observed in well-developed fogs.

The liquid water mixing ratio w can be written

$$w = N \frac{4\pi}{3} \frac{\rho_l}{\rho} r^3 \tag{35}$$

where N is the number of drops per unit volume, r is the mean volume radius of the drop-size distribution, ρ_l is the density of liquid water, and ρ is the air density. Eq. (27) can be solved for r and the result substituted in the Stokes relationship (Fletcher, 1966)

$$V_t = 1.2 \times 10^6 r^2 \text{(cgs units)} \tag{36}$$

for terminal velocity of water droplets under 20 μm in radius. The resulting expression is

$$V_t = 5.3 \times 10^3 \left(\frac{w}{N}\right)^{\frac{2}{3}} \tag{37}$$

where N is number of drops cm^{-3}.

Assuming a constant drop concentration $N = 50\ cm^{-3}$, reasonably representative of coastal advection fogs (Mack et al., 1975), Eq. (37) reduces to the expression

$$V_t = 4 \times 10^2 w^{\frac{2}{3}} \text{ cm/sec} \tag{38}$$

employed in the model. For a liquid water mixing ratio $w = 2.44 \times 10^{-4}$ corresponding to liquid water content of approximately 0.30 g m^{-3}, Eq. (38) yields $V_t = 1.5$ cm sec^{-1}.

Fairly realistic results have been achieved in this study and earlier fog modeling studies (Pilié et al., 1972; Mack et al., 1972) using this parameterization of the influences of fog drop sedimentation on fog development. However, since the drop sedimentation term has been demonstrated to have a large influence on predicted fog development in the model, careful consideration should be given to a better description of fog drop sedimentation in future fog modeling studies. The description of fog drop sedimentation in the model might be significantly improved by carrying out even-highly parameterized microphysical calculations in the model.

- Horizontal Advection

The horizontal advection terms in the differential Eqs. (1) through (5) are approximated in the model by upstream differences which have the form

$$u \frac{\partial Q}{\partial x} = u_{i,k} \left(\frac{Q_{i,k} - Q_{i-1,k}}{x_i - x_{i-1}} \right) \tag{39}$$

for $u_{i,k} \geq 0$.

When combined with forward time differencing, this finite-difference scheme is computationally stable when

$$u \frac{\Delta t}{\Delta x} \leq 1 \tag{40}$$

Thus, the maximum value of u and the minimum value of the horizontal grid length Δx determine the maximum value of the time step Δt for which the integration will be stable. If u_{max} = 6.0 m sec and Δx_{min} = 1000 m, then Δt_{max} ≈167 sec.

The upstream differencing scheme has well-known pseudo-diffusive properties (Molenkamp, 1968), which can be expressed in terms of a horizontal pseudo-diffusion coefficient

$$\nu_H = \frac{1}{2}|u|\Delta x(1 - u\frac{\Delta t}{\Delta x}) \tag{41}$$

No unique value can be assigned ν_H in the model because u varies in the vertical and Δx varies in the horizontal in the expanding portions of the horizontal grid. Above a few meters height, however, ν_H generally exceeds $10^2 m^2 sec^{-1}$ in the numerical experiments to be discussed. This results in the rapid damping of short wavelength disturbances in the horizontal. While this property of the finite difference scheme would be particularly unattractive in studies of transient solutions, it is not without advantage in the study of forced, steady-state solutions, particularly if the present model is generalized in the future by the incorporation of prognostic fluid dynamic equations.

2.2.3 Initial Conditions

At each vertical grid level in the two-dimensional advection fog model, the initial values of the prognostic variables Θ, r, w, u, and v are normally uniform in the horizontal. The model permits initialization with any vertical distributions of the prognostic variables. In the fog formation cases to be discussed, the model was initialized with vertical distributions generated by allowing a one-dimensional (in z) version of the model to evolve to approximately steady-state above an ocean surface about 12 hours after being initialized with some simple theoretical vertical distributions of the prognostic variables. These initial vertical distributions generated by the one-dimensional model can be thought of as corresponding to an air mass which has been conditioned by a significant trajectory over a uniform ocean surface.

For testing purposes and simple fog formation simulations, the advection fog model is easily initialized with certain idealized vertical distributions of the prognostic variables. The initial distribution of potential temperature can be either adiabatic (Θ = constant) or correspond to an isothermal temperature distribution. The water vapor mixing ratio can be

initialized with a uniform distribution with height. The liquid water mixing ratio w can be initialized to be zero everywhere. The u component of the horizontal wind can be initialized to have a logarithmic height dependence of the form $\ln(\frac{z + z_0}{z_0})$. The v component of the horizontal wind can be initialized to have a logarithmic height dependence near the surface, but to approach zero at the upper boundary.

2.2.4 Boundary Conditions

In the numerical experiments to be discussed, the water vapor mixing ratio at the surface was maintained equal to the saturation mixing ratio at the temperature of the surface. This boundary condition was applied to study fog formation and development over an ocean surface. The liquid water mixing ratio at the surface was maintained equal to zero on the assumption the ocean surface represents a sink for atmospheric liquid water. At the surface, both the u and v components of the horizontal wind were set to zero.

The basic objective in fog formation and other numerical experiments with the advection fog model is to study the response of the model to discontinuities in the surface temperature. Since the initial condition is a uniform surface temperature, the surface temperature discontinuities are introduced gradually over the first 30 minutes of the numerical experiments to avoid sudden pulsing of the model at the start of an integration. The model allows any structure of the surface temperature to be introduced.

The upper boundary of the grid system at approximately one kilometer height is assumed to be an undisturbed level. There, the prognostic variables are maintained equal to their initial values throughout a numerical experiment. The value of the u component of the horizontal wind at the upper boundary is assumed to be the geostrophic wind u_g in the equation of motion for the v component. The v component of the horizontal wind at the upper boundary is correspondingly maintained equal to zero.

At the upwind boundary of the grid system, the normal boundary condition is to maintain the prognostic variables equal to their initial values during an integration. At the downwind boundary, the values of the prognostic variables are continually adjusted to be equal to the computed values in the adjacent upwind column of the grid system. While there is no mechanism for upwind propagation of information in the present model, this procedure was adopted with an eye to eliminating reflections of gravity waves at the downwind boundary if the model is generalized in the future by incorporation of dynamic process.

2.2.5 Computational Procedure

- Grid System

In the vertical grid employed in the model, the spacing between adjacent grid levels expands upward from the surface. The expanding grid system provides high resolution near the surface where the variables of the model change rapidly with height and removes the upper boundary from the region of primary change, without requiring a prohibitively large number of grid levels. In the numerical experiments to be discussed, 43 grid levels have been employed with the grid spacing expanding upward by a factor of 1.2 per level from an initial spacing of 10 cm between the first grid level in the atmosphere and the surface. The upper boundary was 205 m above the next highest grid level and 1060 m above the surface.

In the horizontal grid system, the grid expands both upwind and downwind about an interior region with uniform grid spacing. Within the limitation of a maximum of 40 horizontal grid columns, the model permits great flexibility in specifying the horizontal grid parameters for different applications.

- Implicit Integration

Since the vertical grid has very fine grid spacing near the surface, it was necessary to adopt an implicit treatment of the vertical diffusion terms in the partial differential equations of the model (Eqs. (1) - (5)) in order to obtain computationally stable solutions using reasonably large time steps.

Omitting the symbolic source term C for condensation, the finite-difference equations employed in the model can be written in the form

$$\frac{\Theta^{n+1} - \Theta^{n}}{\Delta t} = -u^{n} \frac{\delta \Theta^{n}}{\delta x} + \frac{\delta}{\delta z}\left(K_h^{n} \frac{\delta \Theta^{n+1}}{\delta z}\right) - \frac{1}{\rho C_p}\left(\frac{1000}{p}\right)^{\frac{2}{7}} \frac{\partial R^{n}}{\partial z} \tag{42}$$

$$\frac{r^{n+1} - r^{n}}{\Delta t} = -u^{n} \frac{\delta r^{n}}{\delta x} + \frac{\delta}{\delta z}\left(K_h^{n} \frac{\delta r^{n+1}}{\delta z}\right) \tag{43}$$

$$\frac{w^{n+1} - w^{n}}{\Delta t} = -u^{n} \frac{\delta w^{n}}{\delta x} + \frac{\delta}{\delta z}\left(K_h^{n} \frac{\delta w^{n+1}}{\delta z}\right) + \frac{\delta\left(V_t^{n} w^{n+1}\right)}{\delta z} \tag{44}$$

$$\frac{u^{n+1} - u^{n}}{\Delta t} = -u^{n} \frac{\delta u^{n}}{\delta x} + \frac{\delta}{\delta z}\left(K_m^{n} \frac{\delta u^{n+1}}{\delta z}\right) + f \cdot v^{n} \tag{45}$$

$$\frac{u^{n+1} - u^{n}}{\Delta t} = -u^{n} \frac{\delta u^{n}}{\delta x} + \frac{\delta}{\delta z}\left(K_m^{n} \frac{\delta v^{n+1}}{\delta z}\right) + f \cdot (u_g - u^{n}) \tag{46}$$

where n and n + 1 denote values known at the end of successive time steps. Thus, the horizontal advection terms, the radiative flux divergence $\frac{\partial R}{\partial z}$, the exchange coefficients K_m and K_h, the mean terminal velocity of the fog drops V_t, and the Coriolis terms in the horizontal wind equations are computed from the known values of the prognostic variables at the end of the previous time step n. The prognostic variables in the vertical diffusion terms and w^{n+1} in the drop sedimentation term are the new values to be determined at the end of time step n + 1.

The method of solution of these implicit finite-difference equations of the advection fog model by the technique of Richtmyer (1957) is outlined in the discussion of an earlier version of the model by Mack et al. (1972). The implicit integration method and the computational sequence employed in the advection fog model are fundamentally unchanged by the incorporation of the prognostic equations for the horizontal wind and other improvements to the model accomplished during this investigation. The reader is, therefore referred to the report by Mack et al. (1972) for a discussion of the numerical integration method used in the advection fog model.

2.3 APPLICATION OF THE MODEL

2.3.1 Introduction

Numerical modeling studies are at least two-part projects. One is the task of developing a reasonable mathematical description of the physics of the problem and a stable, accurate numerical representation of that mathematical description. The other consists of applying the model to the phenomena under study and interpreting the results. Of fundamental importance to both tasks is a concept of how the phenomenon forms and develops. In addition to describing the physics involved, it is necessary to provide a combination of realistic initial and boundary conditions from which the phenomenon can evolve. These concepts develop through combined field investigations and theoretical modeling studies.

The original development and testing of the Calspan advection fog model (Mack et al., 1972) was carried out under woeful lack of observational information. Since 1972 Calspan has conducted observational studies of marine fog off the coast of California, which can provide guidance for the development and application of numerical fog models. These studies have demonstrated that marine fog forms and develops by a variety of mechanisms (Mack et al., 1975). One observed mechanism, stratus lowering, was simulated in a numerical modeling study of marine fog by Barker (1973). In the present study, the

advection fog model has been applied to simulate the formation of marine fog by boundary layer exchange processes, which result when nearly saturated air is advected over a change in water temperature. In the marine fog program, local fogs have been observed to form when nearly saturated air was advected over warmer water. Since the representation of vertical turbulent exchange in the model precluded the proper simulation of fog formation by the advection over warmer water, the formation of marine fog by advection of nearly saturated air over colder water was investigated with the advection fog model. Where possible, the marine fog observations were used to guide the investigation and delineate important areas for future improvement and application.

The present study is directed at investigating marine fog formation in response to water temperature discontinuities. In order to assure that the simulations with the advection fog model would respond soley to this type of surface forcing, upwind vertical distributions of the model variables were employed which were very nearly in steady-state equilibrium with each other and the upwind surface temperature. These upwind distributions were generated by initializing a one-dimensional version of the model with some idealized vertical distributions of the variables, and by running the model until the vertical distributions evolved to a quasi-steady state, compatible with the boundary condition aloft and the simulated ocean boundary conditions at the surface. In this manner, upwind distributions were employed in the advection fog model which were representative of air which had been conditioned by a significant trajectory over a uniform ocean surface. These distributions were advected over decreases in surface temperature in the advection fog model to investigate the formation of marine fog by that process.

2.3.2 Fog Formation by Mixing

To simulate marine fog formation as a result of water temperature discontinuities, it is assumed in the model that the boundary condition on the water vapor mixing ratio at the surface is saturation at the surface temperature. Downwind from a decrease in surface temperature, saturated air at the new surface temperature is mixed with warmer, nearly saturated air

advecting over the surface temperature decrease. It is this mixing process which is responsible for initial fog formation in the advection fog model. The water temperature decrease that can produce a fog by the mixing process can be determined from the upwind conditions with the aid of a saturation mixing ratio vs. temperature curve in a manner first described by Taylor (1917) and illustrated in Figure 1.

In reference to Figure 1, assume that the upwind air advecting over a decrease in water temperature is at temperature T and at dew point T_D. Let this air mix with saturated air at temperature T_1 over the surface downwind of temperature decrease. If heat and water vapor are mixing in an identical manner, as in the advection fog model where the turbulent exchange coefficients for heat and water vapor are assumed to be equal, all points lie on a straight line between the unmodified upwind air and the saturated surface air downwind of the temperature decrease. In this case, the mixing process does not produce supersaturation and fog cannot form. If the downwind water temperature is T_3, however, significant supersaturation is produced by the mixing process and fog will form. Supersaturation is produced in the mixing zone at all downwind water temperatures colder than T_2, the temperature at which a straight line passing through the point defined by the upwind conditions is tangent to the saturation mixing ratio curve. Any water temperature decreases smaller than $T-T_2$ will result in no fog formation by the mixing mechanism. It is possible, therefore, from such arguments to estimate the minimum change in a surface temperature required to produce a fog in the advection fog model for given upwind conditions, i.e., temperature and dew point.

2.3.3 Upwind Boundary Conditions for Two-Dimensional Simulations

Consideration of fog formation by mixing indicates that the dew point depression upwind of a sea surface temperature discontinuity determines whether fog will form as a result of advection over the discontinuity in surface temperature. For a pure water surface, it is predicted from mixing arguments that the dew point depression, upwind of an $8^{o}C$ decrease in surface

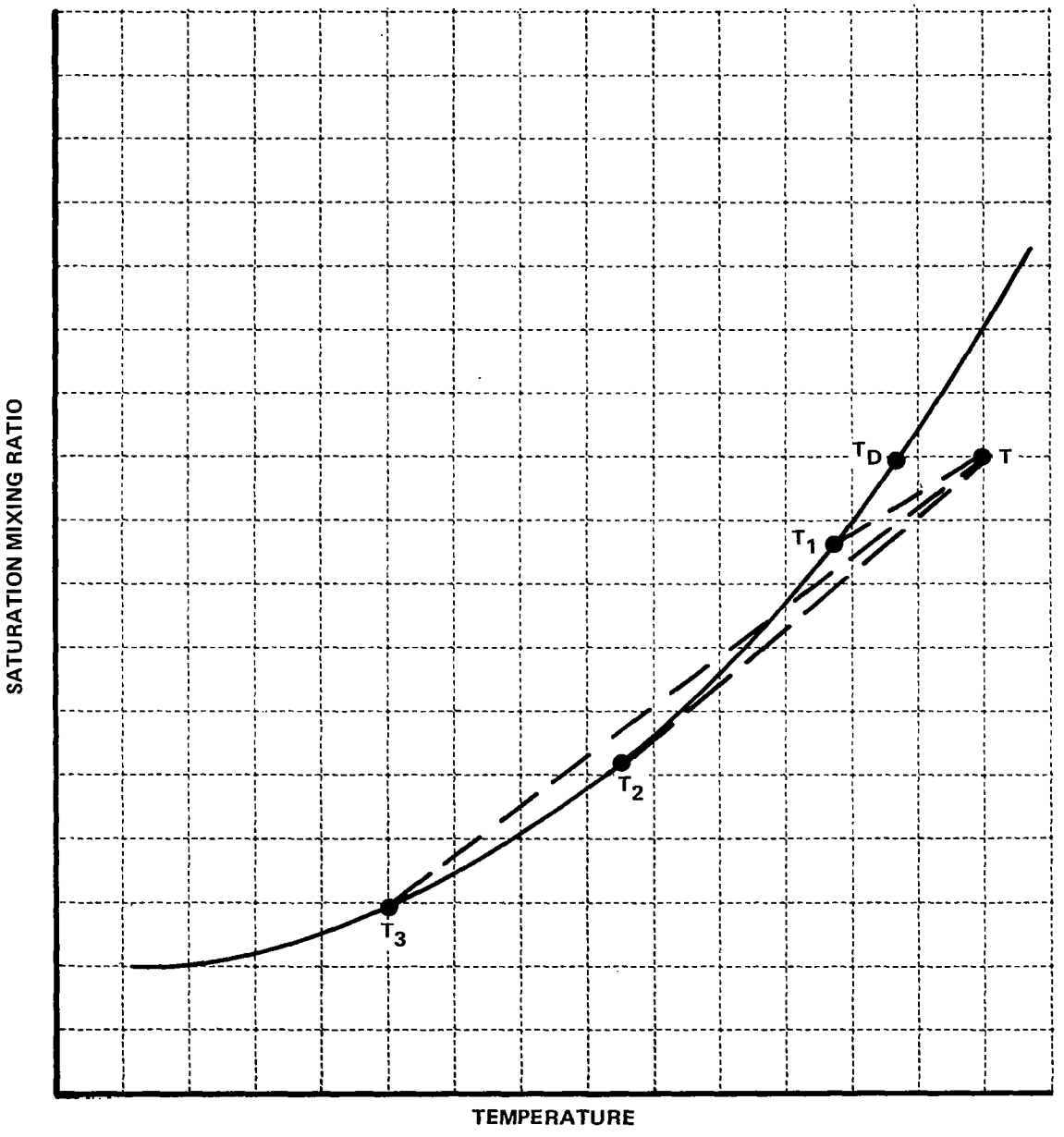

Figure 1 SCHEMATIC CURVE OF SATURATION MIXING RATIO VS TEMPERATURE

temperature, must be 0.5°C or less for fog formation. It is apparent that careful consideration of upwind dew point depressions is required in order to obtain reasonable results in two-dimensional numerical simulations of marine fog formation by cooling.

Ideally, upwind boundary conditions should be vertical profiles of temperature and moisture which were observed in air which later experienced fog formation. Such observations, in particular those of moisture, do not exist. The approach used in this study was to generate upwind boundary conditions by running the numerical model in a one-dimensional mode to simulate the long overwater trajectory. There were two advantages to this method. One, the upwind boundary conditions for the two-dimensional model were in mutual adjustment throughout the model depth, i.e., the profiles of the prognostic variables were in balance with the profile of the turbulent exchange coefficient. Two, the moisture profile was generated from the surface boundary condition of saturation.

Running the model in a one-dimensional form still required initial conditions. In July 1973 Calspan took aircraft soundings 50 n mi out to sea northwest of Vandenberg AFB in California. These observations were taken in a 400-600 m thick boundary layer with stratus present in the upper portion. Below the base of the stratus cloud, the temperature profile was adiabatic indicating well-mixed conditions. The moisture profile also indicated well-mixed conditions. These observations suggested that a well-mixed layer might be a reasonable initial condition for the one-dimensional simulations.

When one-dimensional simulations were initialized with a uniform potential temperature equal to the surface temperature, the temperature distribution did not change with time. The water vapor mixing ratio was initialized to constant values near the surface corresponding to a few degrees Celsius dew point depression. Aloft the mixing ratio was decreased to avoid initial supersaturation. As a result of the saturation boundary condition on the mixing ratio at the surface, evaporation occurred and the mixing ratio increased

with time in the course of one-dimensional simulations. Because of the rapid decrease of temperature with height, stratus formation eventually occurred unless initial mixing ratios aloft were very small.

Although stratus formation and the lowering of stratus to the surface under the influences of radiation cooling is an important mechanism of marine fog formation off the California coast (Mack et al., 1975), the objective of the present investigation was to examine the triggering of marine fog formation by advection of nearly saturated air over water temperature discontinuities. It was concluded that, while the well-mixed initial condition on temperature was conducive to stratus formation in the one-dimensional simulations, it was not conducive to the production of nearly saturated conditions near the surface.

To obtain smaller dew point depressions near the surface and, at the same time, avoid stratus formation, one-dimensional simulations were initialized with an isothermal temperature profile. However, because of an initial imbalance between the isothermal profile and the profile of turbulent exchange coefficient, the eddy heat flux showed both convergence and divergence. With convergence in the lower levels and divergence around 100 m, the isothermal profile evolved to nearly an adiabatic profile from the surface up to 100 m. Above 100 m the profile remained isothermal at the original temperature. One of these one-dimensional simulations produced a dew point depression of $0.323^{o}C$ at the surface with a second minimum of $0.2^{o}C$ at the top of the adiabatic layer.

When these steady-state conditions were used to initialize a two-dimensional simulation, numerical stability problems appeared with the Richardson number formalism for the turbulent exchange coefficients. After much work to eliminate this instability proved fruitless, the Richardson number formalism was abandoned and a constant flux approach was adopted which used surface heat flux to specify the stability. With the constant-flux formalism, small values of the turbulent exchange coefficients developed in the model above fog formed by cooling the air from below. Consequently, study of the complete development of this type of fog to large depths was no longer feasible. However, both fog formation in the surface layer and the early stages of fog development could be studied.

2.3.4 Fog Formation by Cooling from the Surface

Starting from an isothermal profile, a one-dimensional simulation, which used the surface heat flux formalism for the turbulent exchange coefficients, produced a slightly lapsed temperature profile with approximately $0.4^{o}C$ difference between the surface and 100 m. The dew point depression was $0.5^{o}C$ near the surface and increased to $1.0^{o}C$ at 300 m. The saturation mixing ratio vs. temperature curve indicated that a temperature decrease of at least $8^{o}C$ would be needed to form fog with the $0.5^{o}C$ dew point depression. In a two-dimensional simulation, these upwind boundary conditions were advected over a surface which was $8^{o}C$ colder than the upwind surface temperature. The horizontal dimension of the colder water was 20 km. At the wind speeds involved in the lowest levels (~1.5 m/sec), a four-hour simulation was needed to set up a steady state throughout the 20 km horizontal extent of the model.

At the extreme downwind location, a 9 m deep fog formed with an average liquid water content (LWC) of 0.15 g/m^{3}. Due to the large decrease in surface temperature, the air temperature profile was strongly inverted, with 40 m being the height at which no cooling had taken place. Between the surface and 40 m, the temperature difference was $6.6^{o}C$ producing a mean gradient of $0.165^{o}C/m$ through the layer. This gradient was an order of magnitude greater than that in the inversion observed by Taylor (1917) in the low levels of fog off Newfoundland. In an attempt to bring the strength of the inversion produced in the model fog closer to the observed inversion, a smaller temperature decrease of $-4^{o}C$ was used. From the mixing argument for a $-4^{o}C$ temperature change, a surface dew point depression of $0.25^{o}C$ would be needed as the upwind condition.

To obtain very small dew point depressions in the one-dimensional model, u* was decreased to 5 cm/sec to reduce the heating resulting from the initial imbalance associated with the isothermal profile. Without this reduction, the model could not produce dew point depressions under $0.3^{o}C$. The temperature profile shown in Figure 2 was obtained from the one-dimensional model in this mode; the corresponding dew point depression was $0.167^{o}C$ at the surface.

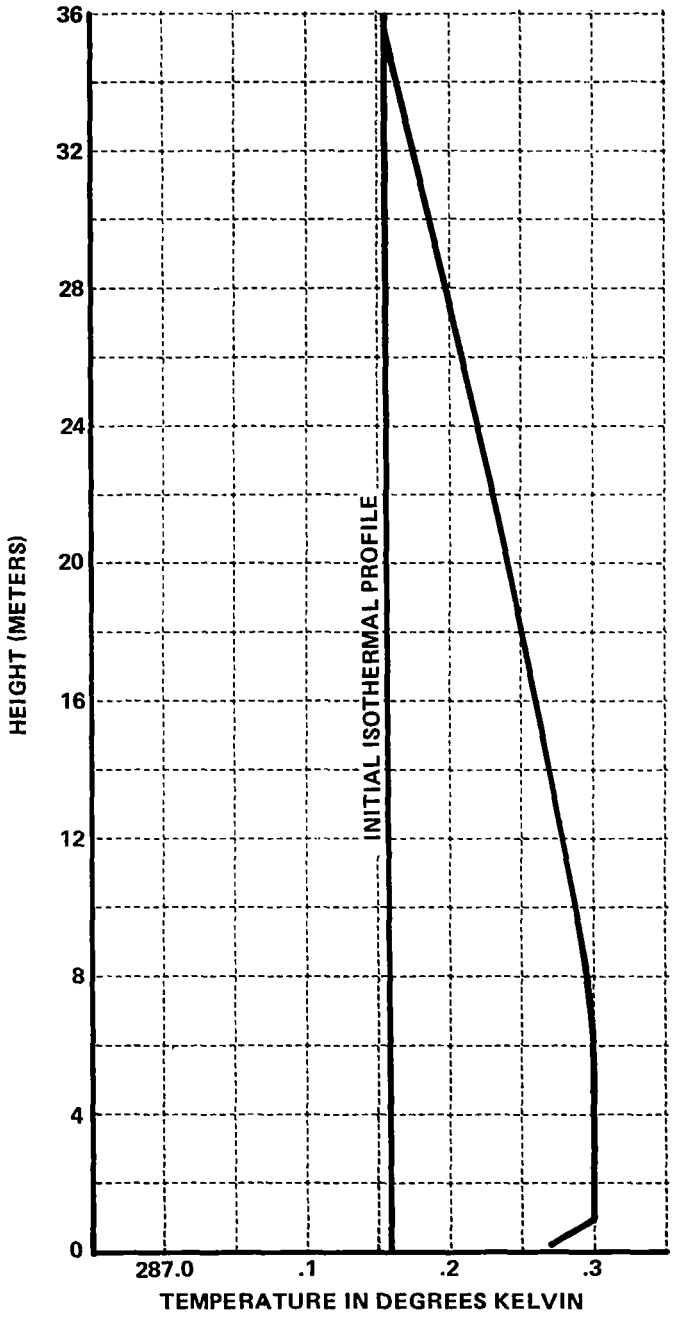

Figure 2 STEADY STATE TEMPERATURE PROFILE GENERATED BY ONE-DIMENSIONAL SIMULATION

Because of the smaller wind speeds at the lower levels (0.75 m/sec), only 10 km was needed in the horizontal to encompass the steady-state conditions after four hours. The steady-state fog at 10 km was only five meters deep with LWC equal to 0.1 g/m^3 confined to below 1 m. The cooling was confined to 20 m and below. The temperature difference between the surface and 20 m was 3.5°C producing a gradient of 0.175°C/m, the same magnitude as in the -8°C case. Although the cooling in the boundary layer was proportional to the change in the surface temperature, the cooling was confined to a shallower layer, so that the temperature gradient in the inversion remained essentially the same. The discrepancy between the model results, and Taylor's measurements may lie in the measurements. Modern, more detailed measurements are scheduled to be taken in fog situations off Newfoundland in the summer of 1975. These measurements should provide better observations for comparison with the model results.

In summary, the model results show heat loss to a cooler ocean surface at saturation can produce fog formation, but because of the real boundary condition of saturation over a salty ocean, an initial dew point depression of about 0.25°C requires a 6.5°C change in the surface water temperature. Measurements off the California coast have shown that changes of this magnitude in the surface water temperature are not required where fog actually forms. Apparently some process, other than loss of heat to the sea surface, is responsible for formation of fog under these circumstances. However, it is likely that such large temperature discontinuities may exist on the north side of the Gulf Stream, an area scheduled for field investigation in the summer of 1975. If fog is found to form there under large decreases in sea surface temperature, determination of whether the fog forms by cooling will require accurate measurement of humidities near saturation.

2.3.5 Effect of Drop Sedimentation on Fog Growth

Although the model fogs formed above did not grow to large depths, some insight into the effects of drop sedimentation and turbulent intensity

on fog growth can be obtained by comparison of the two simulations. A comparison of the two steady-state fogs is shown in Table I.

Table I.

COMPARISON OF STEADY-STATE FOG PROPERTIES FOR $-4^{o}C$ and $-8^{o}C$ SURFACE TEMPERATURE CHANGES

	Fog Top Height (m)	Turbulent Exchange Coefficient at Fog Top (cm^2/sec)	Characteristic Liquid Water Content (g/m^3)
$-4^{o}C$	4.85	37.7	<0.1
$-8^{o}C$	8.74	267	>0.1

For the fog with the higher top, the turbulent exchange coefficient is about six times larger than that with the lower fog. Larger K's were present at the fog top not only at 20 km, but at all locations between 20 km and the upwind boundary. The higher K's in the $-8^{o}C$ case arose from higher K's in the upwind condition. Qualitatively, it might be expected that in the case with the larger K's the fog might grow to higher heights than it did. However, the sedimentation is larger in the $-8^{o}C$ case. In the $-8^{o}C$ case, the fog drops fall at approximately 1 cm/sec, while in the other case they fall at approximately 0.5 cm/sec. Thus, in the $-8^{o}C$ case, the promoting and inhibiting processes for fog growth are both larger, with the net effect being only a slightly higher fog.

Further insight into the control of fog development by sedimentation was obtained by running a simulation in which the only change was elimination of the sedimentation. This type of simulation was run for the conditions of the $-4^{o}C$ case, and the fog grew to 70 m in depth at the 10 km location. However, this growth was not entirely due to absence of sedimentation. The turbulent exchange coefficients were also larger. In the model, the strength of the K's is related to the liquid water content through the radiative cooling.

If larger liquid water is present over greater depths, less stable temperature profiles are produced and, hence, strong turbulence occurs. However, the K's in the simulation without sedimentation were the same order of magnitude as those in the -8°C case, in which fog grew only to 9 m. Therefore, the major effect on fog development was the absence of sedimentation. Since sedimentation has such a profound effect on fog development, the fall velocity of drops must be modeled carefully in any numerical simuations designed to study fog growth.

2.3.6 Growth of Shallow Fog Over Warmer Water

The modeling work has shown that fog formation is possible over the ocean by cooling in a shallow layer near the ocean surface. However, the large discontinuities in surface water temperature that are required have not been found in the observations of fog occurrence over the open ocean west of California. Analysis of that field data (Mack et al., 1975) lead to the following description of fog formation and development by processes other than cooling from the surface:

> "Local fogs have been observed to form in cool, nearly saturated air advecting over warmer water. Subsequent turbulent exchange and enhanced evaporation from the sea surface lead to mixing of warm, moist surface air with cool, moist air at higher levels and initial condensation in a shallow layer. Radiative cooling of this thin layer lifts the inversion base from the sea surface and further fog development is promoted by radiative cooling and enhanced mixing beneath the locally induced, low-level inversion."

The capabilities of the numerical model were utilized to examine the feasibility of fog development by these processes. The simulation involved moving a shallow fog (formed by previous cooling) over warmer water to determine the effect on fog thickness.

The experiment design was as follows. A 7 m deep fog, which had been generated by a water temperature decrease of 4°C, was used as upwind

boundary conditions for a two-dimensional simulation. These conditions were advected over a water temperature which was 2°C warmer than that which the air previously had been exposed to. A control experiment was run in which the same boundary conditions were moved over water at the same temperature to which the air had been exposed for the previous four hours.

In the heating case the fog top grew to 18.7 m compared to a height of 8.75 m in the continued cooling case. Exposure to heating raised the fog top height to a level more than twice that which occurred with continued cooling. One reason for the difference was the increased turbulent intensity at the fog top as the air moved over warmer water. In the heating case, the turbulent exchange coefficients at and above the fog top were an order of magnitude larger than those in the continued cooling case. Thus, the increased turbulence moved the fog top upward by diffusion of both the liquid water and the cooling produced by radiation at the fog top. However, an attempt to develop a deeper fog by increasing the temperature difference to 3°C led to complete evaporation of the fog. As with most parameters involved with fog formation, the small change in water temperature increase had a drastic impact on the fog behavior.

The upwind temperature profile and the temperature profiles through each of the two fogs are shown in Figure 3. In the cooling case, the temperature shows a small decrease uniformly distributed below 20 m, thus maintaining the strongly inverted temperature profile. On the other hand, in the warming case, temperature increases up through 7 m and decreases from there up through 30 m. The initial inversion of 3.5°C between the surface and 20 m is reduced to a little more than a degree. In this case, the maximum cooling located around 14 m is associated with radiational cooling which extends up to the fog top at 18.7 m (Figure 3). This result indicates the importance of radiational cooling to fog development as hypothesized by Mack et al. (1975).

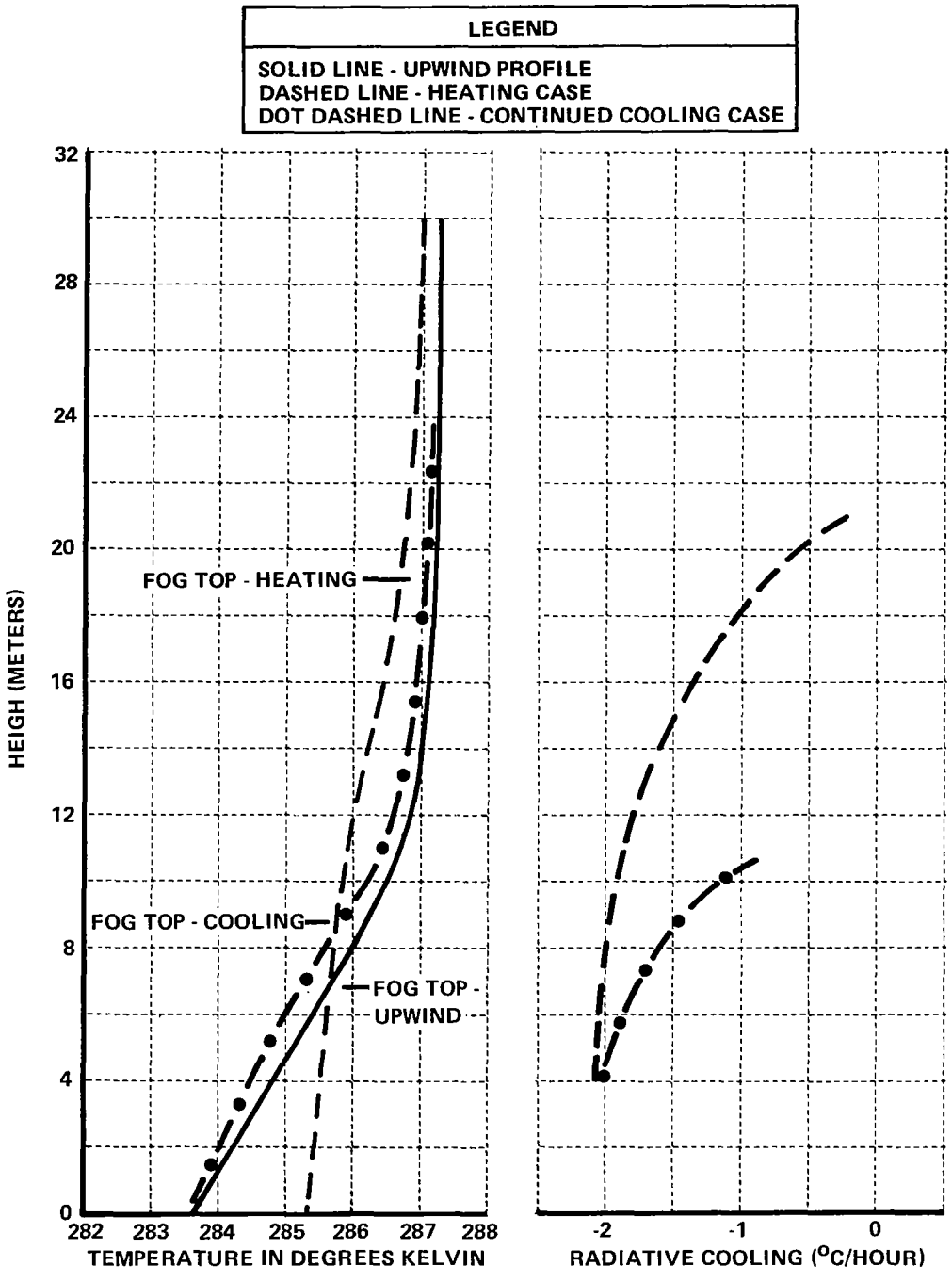

Figure 3 VERTICAL PROFILES OF TEMPERATURE AND RADIATIVE COOLING IN FOG EXPOSED TO 1) CONTINUED COOLING AND 2) HEATING

2.4 CONCLUSIONS AND RECOMMENDATIONS

In this study, a two-dimensional numerical model of advection fog was improved by incorporation of prognostic equations for the horizontal wind and by utilizing both the predicted wind and potential temperature distributions to determine the turbulent exchange coefficients in the model. Numerical simulations of advection fog formation and development over an ocean surface were compared with Calspan's observations of marine fog off the California coast. When air which had been conditioned by simulation of a significant trajectory over a uniform ocean surface was subjected to a decrease in surface temperature, the advection fog model predicted that a surface temperature decrease on the order of $4^{o}C$ or larger was required for fog formation. Calspan's observations of marine fog formation in such a conditioned air mass, however, indicate that fog formation occurs with surface temperature changes of about $1^{o}C$. In addition, the subsequent vertical development of fog is often significantly greater than that predicted by the advection fog model.

Since the advection fog model is a boundary layer model in which it is assumed that turbulent exchange coefficients for heat and water vapor are equal, there are at least two possible explanations for the apparent discrepancy between the requirements for fog formation in the advection fog model and in the real atmosphere. One possibility is that mesoscale circulations induced by advection over surface temperature changes, which are neglected in the advection fog model, may promote fog formation in the real atmosphere. Calspan's observations indicate that mesoscale convergence can be an important element in the development and persistence of coastal fog (Mack et al., 1975). A second possible explanation is that the transfer of heat and water vapor between ocean and atmosphere in response to changes in the ocean surface temperature may proceed at slightly different rates, promoting fog formation under certain circumstances. Indeed, Fukuta and Saxena (1973) have argued that the greater rate of molecular diffusion of water vapor than of heat in the laminar sublayer at the ocean surface aids fog formation over warmer water and inhibits fog formation over colder water. In addition, if the turbulent

exchange coefficients for the vertical transfer of heat and water vapor are slightly different, a similar type of rate dependent (kinetic) effect on fog formation would result.

While the incorporation of dynamic influences into the advection fog model is an important objective, there appears to be sufficiently unresolved questions concerning possible kinetic influences on fog formation and the influences of turbulent transfer on vertical development of fog to justify additional research with the advection fog model in the boundary layer form. It is recommended, therefore, that a numerical modeling investigation should be carried out of possible kinetic influences on advection fog formation over the ocean, using Calspan observations of marine fog formation to guide the study. In order to facilitate this investigation and to develop a better modeling framework for simulating the vertical development of advection fog under the influences of radiative cooling, it is further recommended that a more physically realistic closure for turbulent transfer be incorporated into the advection fog model. This could take the form of incorporating a prognostic equation for the turbulent energy and assumed proportionalities between the turbulent fluxes and the turbulent energy (Pepper and Lee, 1974). Alternatively, a prognostic equation for the turbulent exchange coefficients themselves could be incorporated into the model (Nee and Kovasnay, 1969).

2.5 REFERENCES

Barker, E.H., 1973: Oceanic Fog, A Numerical Study. Technical Paper No. 6-73, Environmental Prediction Research Facility, Naval Postgraduate School, Monterey, California 93940.

Businger, J.A., J.C. Wyngaard, Y. Izumi, and E.F. Bradley, 1971: Flux-Profile Relationships in the Atmospheric Surface Layer. J. Atmos. Sci., 28, 181-189.

Fletcher, N.H., 1966: Physics of Rainclouds. Cambridge University Press, 389 pp.

Fukuta, N. and V.K. Saxena, 1973: Kinetic Threshold Conditions for Fog Formation in Cloud Chambers and Marine Environment, J. Atmos. Sci., 30, 1638-1644.

Goody, R.M., 1964: Atmospheric Radiation. Oxford University Press, 436 pp.

Hsu, S.A., 1974: On the Log-Linear Wind Profile and the Relationship Between Shear Stress and Stability Characteristics Over the Sea. Boundary-layer Meteor., 6, 509-514.

Korb, G., and W. Zdunkowski, 1970: Distribution of Radiative Energy in Ground Fog. Tellus, 22, 298-320.

Lumley, J.L., and H.A. Panofsky, 1964: The Structure of Atmospheric Turbulence. New York, Interscience Publishers, 239 pp.

Mack, E.J., W.J. Eadie, C.W. Rogers, W.C. Kocmond, and R.J. Pilie, 1972: A Field Investigation and Numerical Simulation of Coastal Fog, Calspan Report No. CJ-5055-M-1, Calspan Corporation, Buffalo, N.Y. 14221.

Mack, E.J., U. Katz, C.W. Rogers, and R.J. Pilié, 1974: The Microstructure of California Coastal Stratus and Fog at Sea, Project SEA FOG: Second Annual Summary Report, Calspan Report No. CJ-5404-M-1, Calspan Corporation, Buffalo, N.Y. 14221.

Mack, E.J., R.J. Pilié, and U. Katz, 1975: Marine Fog Studies Off the California Coast, Project SEA FOG: Third Annual Summary Report, Calspan Report No. CJ-5067-M-1, Calspan Corporation, Buffalo, N.Y. 14221.

McDonald, J.E., 1963: The Saturation Adjustment in Numerical Modeling of Fog, J. Meteor., 20, 476-489.

Molenkamp, C.R., 1968: Accuracy of Finite-Difference Methods Applied to the Advection Equation. J. Appl. Meteor., 7, 160-167.

Nee, V.W. and L.S.G. Kovasnay, 1969: A Simple Theory of the Turbulent Shear Flows, Phy. of Fluids, 13, 473-484.

Panofsky, H.A., 1974: The Atmospheric Boundary Layer Below 150 Meters. Ann. Rev. Fluid Mech., 6, 147-177.

Pepper, D.W. and S.C. Lee, 1974: Transport Phenomena in Thermally Stratified Boundary Layers, Proc. AIAA/ASME Thermophysics and Heat Transfer Conference, July 15-17, 1974, Boston, Mass.

Pilié, R.J., W.J. Eadie, E.J. Mack, C.W. Rogers, and W.C. Kocmond, 1972: Project Fog Drops, Part I -- Investigation of Warm Fog Properties, Calspan Report No. RM-3005-M-5, Calspan Corporation, Buffalo, N.Y.

Richtmeyer, R.D., 1957: Difference Methods for Initial-Value Problems. Interscience Publishers, 238 pp.

Shir, C.C., 1973: A Preliminary Numerical Study of Atmospheric Turbulent Flows in the Idealized Planetary Boundary Layer. J. Atmos. Sci., 30, 1327-1339.

Sutton, O.G., 1953: Micrometeorology, New York, McGraw Hill, 333 pp.

Taylor, G.I., 1917: The Formation of Fog and Mist, Quart. J. Royal Meteor. Soc., 43, 241-268.

Zdunkowski, W.G., and B.C. Nielsen, 1969: A Preliminary Prediction Analysis of Radiation Fog, Pure and Appl. Geophys., 75, 278-299.

Section 3

RECOMMENDATIONS FOR SIMPLIFIED INDIVIDUAL ZERO-GRAVITY CLOUD PHYSICS EXPERIMENTS

3.1 INTRODUCTION

The following brief discussion is intended to develop recommendations to NASA for selected cloud physics experiments applicable to zero-gravity conditions. As outlined in the work statement, the basic criteria for the selection of the experiments are, first, their pertinence to current fog and fog modification research and, secondly, their simplicity, best described as "carry-on" or "suitcase" experiments.

Preparations for a complex cloud physics laboratory (CPL) intended as a payload for space shuttle sorties have been described recently by Greco et al. (1974) and summarized by Greco and Turner (1975). In cooperation with the cloud physics community, the 20 most promising experiments have been selected and conceptual designs of the experimental setup, including five different cloud chambers, have been created (see Table II). By integrating a multitude of test devices into the CPL, considerable savings are possible and duplication of numerous common components can be avoided. However, since several of the more demanding experiments may require substantial additional development, it would be advantageous to choose a few comparable tests which can be performed with the least elaborate preparation and be developed into simple, individual carry-on kits. This would not only yield early scientific results but also provide further experience which could be applied in the final design of the CPL.

Since a great deal of thought had already been invested in drawing up the list of 20 most desirable experiments, no additional experiments will be taken into consideration here. Rather, we will select from the list of 20 those that fulfill, in our opinion, the aforementioned criteria of being adaptable as carry-on experiments and also have applications to fog physics research.

Table II. SUMMARY OF EXPERIMENT CLASSES
(after Greco et al., 1974)

Experiment Class Number and Title	Primary Chamber*	Alternate Chamber*
1. Condensation Nucleation	CFD	E
2. Ice Nucleation	SDI	E
3. Ice Multiplication	SDI	E
4. Charge Separation	SDI	G
5. Ice-Crystal Growth Habits	SDI	E
6. Scavenging	SDI	G
7. Riming and Aggregation	SDI	G
8. Droplet-Ice Cloud Interactions	SDI	E
9. Homogeneous Nucleation	SDI	E
10. Collision-Induced Freezing	SDI	G
11. Saturation Vapor Pressure	SDI	E
12. Adiabatic Cloud Expansion	E	-
13. Ice Nuclei Memory	E	SDI
14. Terrestrial Expansion Chamber Evaluation	E	-
15. Condensation Nuclei Memory	E	SDL
16. Nuclei Multiplication	G	E
17. Drop Collision Breakup	G	SDI
18. Coalescence Efficiencies	G	SDI
19. Static Diffusion Chamber Evaluation	SDL	-
20. Unventilated Droplet Diffusion Coefficients	SDL	E

*CFD = Continuous-flow diffusion
SDI = Static diffusion, ice
SDL = Static diffusion, liquid

E = Expansion
G = General

Our approach to the experiment selection will proceed in the following sequence: First, a list of experiments relevant to fog will be established; subsequently, this list will be narrowed down on the basis of zero-g applicability. Finally, consideration of equipment problems in view of the simplicity requirement will further reduce the list of eligible experiments.

3.2 PROBLEMS IN FOG MICROPHYSICS

The following brief review of current problems in fog research is intended as a guide for selecting experiments relevant to fog. Although a later section deals with applicability to zero-g, we will limit the discussion at this point to problems in microphysics suitable for experimentation in zero-gravity.

In the initial stages of fog formation, the most important consideration involves the nucleation and subsequent condensational growth of the fog droplets. For a particle of given size and chemical properties, the necessary supersaturation for activation as measured with a thermal diffusion chamber has been found to differ considerably from what theory predicts; e.g., in the case of NaCl, experiments indicate that a 5 times higher supersaturation is required (Katz and Kocmond, 1973), whereas nominally hydrophobic particles have been found to act as condensation nuclei at much lower supersaturations than expected (Ruskin and Kocmond, 1971). At the present time it is not clear whether the discrepancies can be attributed to surface contaminants on the nuclei, to unaccounted for conditions in the cloud chamber or to errors in the particle sizing equipment.

For a given CCN spectrum and cooling rate of the air, it should be possible to accurately predict the ensuing drop size spectrum of the fog. In general, however, calculations of drop size distributions in clouds are in poor agreement with actual observations. In particular, there have only been a very limited number of case studies (see, e.g., Fitzgerald, 1972) where actual measurements of drop sizes and nucleus concentrations at cloud base have been compared with computed values. Although agreement was encouraging with regard

to average drop sizes, discrepancies in the width of the distributions and the total concentrations indicate that important problems still exist. Uncertainties in the measurements point to a need for well-controlled condensation experiments which will provide more reliable data for comparisons with existing models.

In the further evolution of fog (past the early condensational stages), drop sizes may be reached where coalescence starts to play a role. Although this regime is thought to be most important in convective clouds, we have encountered numerous situations where shallow fog (i.e., 200-400 m depth) produced considerable drizzle only conceivable as a result of droplet growth by coalescence. Drizzle has been shown to play an important role in the downward transport of moisture in the evolution of fog from lowering stratus (Mack et al., 1974). Generally, understanding of the coalescence phenomena has progressed considerably in recent years, mainly due to a large number of well-designed wind tunnel investigations at UCLA. The most difficult area of experimentation, i.e., that involving relatively small drops, is the one most applicable to fog; here, further research is needed to compare observations of drop coalescence with theory.

Fog drops not only interact with each other but also with other particles. Since, in most cases, only about 10% or less of all particles act as CCN, those remaining may be scavenged by droplets. The relevance of scavenging to the fog problem can be described as follows: The immediate influence of scavenged particles (or gases) on the host droplet is generally small, except in the case of surfactants which could retard evaporation of the droplet and thus stabilize the fog (see Kocmond et al., 1972). Uptake of salt particles or of gases which react in the liquid phase to produce salts will cause a slight reduction in water vapor pressure over the drop surface in proportion to the increase in concentration of the salt solution. The influence, therefore, will be greater as the droplets evaporate. The most profound effect of particles and gases being scavenged is in the resulting alteration of the CCN spectrum after complete evaporation of the fog droplets has occurred (occasionally referred to as memory effect). Thus, a

subsequent fog formed on the CCN spectrum may possess significantly different microphysical features. This alteration means enlargement of the previously active particles and, in general, a shift of the CCN spectrum to lower critical supersaturations; on the other hand, scavenged surface active substances may have a contrary effect by retarding the nucleation of fog droplets.

A different type of alteration of the CCN spectrum may take place when droplets evaporate completely and the residue breaks up into several smaller particles. The conditions, other than low humidity, under which such a "nuclei multiplication" can occur is not clear at the present time (see Podzimek and Saad, 1974).

Due to the occurence of fogs at subfreezing temperatures, some of the additional problems associated with ice nucleation have to be included in our considerations of experiments suited to zero-gravity conditions. Since most supercooled fogs are stable (i.e., due to a lack of ice nuclei, they usually do not precipitate), ice nucleation enters the picture mainly as a process employed in fog dispersal. The main difficulty in this type of fog abatement scheme is in the economical distribution of suitable ice nuclei (i.e., nuclei that are active at relatively high temperatures). By the preferred use of homogeneously formed ice crystals (dry ice, liquid propane seeding), it is possible to avoid problems of contact nucleation and ice multiplication which are currently among the most debated issues regarding the glaciation of convective clouds.

3.3 RELEVANCE OF EXPERIMENTS TO FOG MICROPHYSICS AND TO ZERO-G APPLICATION

If one examines the list of experiments (Table 1, taken from Greco et al., 1974) in light of the above review of problems in fog microphysics, the following experiment topics seem to be relevant to this research area (in approximate order of importance):

Table III. EXPERIMENTS RELEVANT TO FOG RESEARCH

1. Condensation Nucleation
2. Scavenging
3. Coalescence Efficiency
4. CCN Memory
5. CCN Multiplication
6. Static Diffusion Chamber Evaluation
7. Ice Crystal Growth Habits
8. Ice Nucleation
9. Droplet-Ice Cloud Interactions

From the previous discussion, it is evident that the last three experiment classes are not as important to fog research as the first six topics. The nine experiments shown in Table III are briefly considered below in terms of applicability to zero-gravity tests.

1. Condensation Nucleation: Since droplet growth at low supersaturations (which are typical of fogs) proceeds very slowly, zero-g conditions are especially desirable. As opposed to the situation in the terrestial laboratory, droplets forming on condensation nuclei can be observed for extended times since they will not fall out of the sensitive volume; there are no apparent disadvantages introduced by the weightless conditions.

2. Scavenging: The advantage of studying scavenging under zero-g conditions is two-fold: (1) Elimination of the orthokinetic component will help to identify the effects of other scavenging mechanisms and (2) the lack of droplet sedimentation will allow for interaction with the particles over a time period comparable to actual cloud conditions.

3. Coalescence Efficiency: Droplet coalescence chiefly depends on the motion of the drops relative to the air and to each other. In principle, therefore, strict zero-g conditions present a disadvantage due to the lack of motion; however, by artifically generating a very low gravity situation, relatively large drops can be used to simulate the behavior of the more difficult to work with small cloud droplets (as proposed by Telford, 1974).

4. CCN Memory: Since this effect is essentially a result of scavenging, one has to be aware that at zero-g the potentially considerable orthokinetic scavenging component will be missing. However, the gravity-free environment will permit observation of the same CCN acting before and after uptake of material from the surrounding air.

5. CCN Multiplication: Performance of this experiment would be substantially improved if carried out at zero-g, since one could possibly observe individual CCN before and after shattering instead of merely recording a statistical result as is done in terrestrial tests.

6. Static Diffusion Chamber Evaluation: In the terrestrial laboratory, one of the drawbacks to making CCN measurements at low supersaturations is that the droplets settle out of the sensitive volume before they reach detectable sizes. The extent to which this happens at slightly higher supersaturations must also be determined. The zero-gravity environment offers a unique opportunity to study the fall-out problem and to 'calibrate' the static diffusion chamber for terrestrial use.

7. Ice Crystal Growth Habits: Terrestrial limitations are considerable in this area of research due to the comparatively high fall velocities of ice crystals. Zero-g permits prolonged observation without the need to use supports for growing ice crystals; but, on the other hand, the lack of ventilation presents a serious disadvantage (with the possible exception that it provides one data point for a growth vs ventilation relationship).

8. Ice Nucleation: Most experiments in this category can be carried out successfully in terrestrial chambers due to the generally fast activation of ice nuclei. Zero-g would offer an advantage for testing suspected slow activating ice nucleating aerosols; however, this application would be somewhat less important.

9. Droplet-Ice Cloud Interactions: The interaction between droplets and ice crystals consists of vapor transport from droplets to crystals and droplet-crystal collisions. The first mechanism is basically covered under "ice crystal growth habits", whereas droplet-crystal collisions are largely a result of differences in fall velocities. Thus, the gravity-free environment would only assist in obtaining data from collisions due to such non-gravity effects as, for instance, electrostatic charges.

The experiments considered so far may be further narrowed by eliminating the ice-related topics from Table III. Clearly these are important problems; however, with respect to warm fog microphysics considerations, they are of less relevance.

3.4 LIMITATIONS OF EQUIPMENT TO SIMPLE CARRY-ON APPLICATION

The experiments which were selected so far must also be examined with respect to necessary and available equipment. In the following paragraphs, we therefore review pertinent devices in view of their acceptability for a "simple" setup. The main elements of the equipment in question are: (1) Test chambers for containment of a specific working environment, (2) droplet/particle detectors, and (3) droplet/particle generators.

1. Test Chambers

Although some experiments with hydrometeors such as those conducted aboard Skylab IV (concerning the collison of large water drops; Vaughan and

Hill, 1974) can be performed without the use of confining walls, it is generally necessary to physically define a volume and to control environmental parameters in order to maintain suitable conditions. At the present time, we are in principle not restricted in the choice of cloud chambers as indicated by the findings reported by Greco et al. (1974); however, the basic possibilities are well covered by the five chamber types listed in Table II. The chamber with the most advantages in principle is the expansion type, since in operation uniform temperature changes over the entire volume can be achieved allowing extensive relative humidity variations from fairly dry to high supersaturations. While the expansion chamber provides an excellent simulation of atmospheric situations, its major drawback from the standpoint of our present task (i.e., simple, carry-on equipment) is its complexity in connection with the need to precisely match the wall and air temperature. At this stage of technology, this otherwise ideal chamber is too complicated to be part of a carry-on experiment.

Other chambers for consideration include the thermal diffusion chamber, whose operating principal (diffusion of water and heat from a warmer upper surface to a cooler lower one) allows for a humidity regime adjustable between saturation and a few percent supersaturation. Although these conditions do not provide a true simulation of condensational growth in the atmosphere, they offer the possibility to assess CCN activity. The differences between the three types of diffusion chambers (listed in Table II) currently employed pertain mainly to temperature range and operating mode. In the continuous flow diffusion chamber, CCN are activated while the air sample travels through the chamber; while this may have some advantages where recording of the results is desired, there are two drawbacks: first, the advantage zero-g offers by providing prolonged time for observing droplets is largely cancelled by the motion through the chamber and, secondly, the delicately balanced flow system requires careful adjustment of auxiliary flows making the device rather unsuitable for a simplified carry-on system. In contrast, both static diffusion chambers (liquid surface and ice surface) are operated on the principle that measurements are made in situ, i.e., without removing the sample from the area of supersaturation, thus affording the benefit of zero-g non-fallout. Whereas the chamber with solid (ice) plates may be used for most work on supercooled

clouds, the liquid plate chamber is ideal for typical, warm fog-related investigations. Both chambers stand out by their simplicity, especially the liquid plate version which requires only one temperature control (as opposed to two for the ice plate chamber).

In contrast to expansion and thermal diffusion chambers in which the operating mode provides intrinsically for the formation of hydrometeors, the "general" chamber as described by Greco et al. (1974) constitutes a volume with temperature-controlled walls; it, therefore, needs additional devices for humidification or droplet generation. The apparatus proposed by Telford (1974) for the study of droplet-droplet interactions could be considered a specialized case of the "general chamber" (basically a fall tube in which individual pairs of large droplets (~1/2 mm) are moved under very low gravity (~1/1000 g) simulated by rotation of the apparatus).

From the foregoing discussion, it would appear therefore that the static diffusion chamber with liquid plates is best suited for the simplified carry-on experiments.

2. Droplet and Particle Detectors

The fruitful evaluation of any experiment involving particles and droplets requires some knowledge about their concentration and/or size distribution. When considering fog microphysics, we are mainly dealing with nuclei of 0.01 μm<d<1 μm and droplets in the range 0.5 μm<D<30 μm. It is current laboratory practice to cover the above particle size range with an Electrical Aerosol Analyzer (EAA) and an Optical Particle Counter (OPC; e.g., Royco) for nearly real time results or to examine precipitated particle samples with scanning or transmission electron microscopes. The latter method is very tedious and usually acceptable only for occasional calibrations; also, precipitation of particle samples often introduces additional problems in the analysis.

Both the EAA and the Optical Particle Counter are planned components of the complete CPL, but for our present purposes, the following disadvantages have to be taken into account: Besides the bulk and weight, the EAA depletes aerosol storage due to a relatively high sampling rate (up to 50 liters min^{-1}) and requires higher particle concentrations than generally used in fog-related problems, thus creating a need for a dilution system. The OPC only handles sizes larger than 0.5 μm which makes it unsuitable as the only particle analyzer. An alternate approach to the particle sizing problem will be discussed in the paragraph, "particle generation".

The various methods of assessing cloud droplets also have to be tested for their applicability to a carry-on type of experiment. The optical methods currently used with diffusion chambers (but applicable to others) are direct photography in situ which only records the concentration of drops larger than the sensitivity threshold (e.g., 1 μm), and OPCs which require that the drops be moved from their original location to the analyzer; this latter procedure is quite critical because the slightest change in relative humidity which might occur during transfer will influence the size of the droplets. The above-mentioned photographic method has the advantage over OPCs that sequential exposures can be taken which may contain information about growth rates or which may show the same particle/droplet during several condensation-evaporation cycles. Methods of optical probing in situ (i.e., without disturbing the droplets) by sensing scattered light from a representative sample (as opposed to the drop-by-drop procedure of the OPCs) would be most attractive in principle, but still suffer from interpretative difficulties. A further possibility to assess droplet population is to impact the drops on a sensitive film; this method, however, also removes the droplets from the test volume and disturbs conditions inside the chamber.

If experiments can be designed such that the droplet size does not have to be known accurately (as long as it is above a given value), the photographic method is certainly by far the simplest and most straightforward.

3. Droplet and particle generation

As pointed out previously, droplets are easily formed in expansion and diffusion chambers provided that suitable nucleating particles are present. Thus, the problem is reduced to producing the desired nuclei. Providing small droplets for a "general" chamber will require a droplet generator of a type which yields the particular size spectrum needed for a given application.

Although the study of natural aerosols as they relate to fogs should not be neglected, their complexity makes it difficult to interpret results. Also, storage time during transport into orbit would reduce the value of a natural aerosol considerably. Among the many techniques for producing artificial aerosols, we have to select the ones which utilize simple devices, perform reproducibly and cover the desired size range. In addition, since particle analyzers are impractical for our purpose, we will have to work with a particle generator which produces an accurately predictable size spectrum and concentration--this is practically equivalent to demanding high monodispersity. It is desirable to work with soluble and insoluble particles. Several convenient methods exist for the production of soluble particles from aqueous solutions which are dispersed into droplets and subsequently evaporated. Not all of these methods, however, would be suitable for our purpose; e.g., the dipping reed device has the disadvantage of not producing a high enough concentration. The technique which looks most promising at the present time is the vibrating orifice apparatus where a liquid jet of precisely metered flow is broken into equal segments by a high frequency vibration of the nozzle (see, e.g., Wedding and Stukel, 1974). The commercially available model can produce several hundred particles/cc down to less than 0.1 μm diameter.

Water insoluble particles can be produced with the same device by utilizing a non-aqueous solution of the material in question; however, it may be difficult to remove the solvent from the atmosphere after the solution drops have evaporated. Other methods of generating water insoluble monodisperse aerosols are either too cumbersome for the present purpose (e.g., LaMer generator) or not reproducible enough as in the case of simple evaporation and recondensation.

3.5 RECOMMENDATIONS

From the previous discussion, the following recommendations can be made relative to equipment and experiments for use in a shuttle-type spacecraft.

1. It is recommended that the thermal diffusion chamber be used in initial experiments. The chamber should be equipped with a close-up camera and illumination should be by laser. This apparatus, in conjunction with a vibrating orifice aerosol generator, will allow the following experiments to be carried out:

- Evaluation of static diffusion chamber (SDC). In view of the widespread use of the SDC for measurements of CCN activation spectra throughout the world, it would be especially important to perform an experiment to validate the SDC. This essential task can be accomplished with relatively little effort in the course of initial check out of the equipment at one-g and zero-g. It is recommended that tests be performed to determine the extent of fall out at low supersaturations and that chamber performance be evaluated with several sizes and types of aerosol.

- Condensation nucleation studies: The size-supersaturation relationship for NaCl CCN should be examined carefully in a zero-g environment and, more importantly, extended to larger particles than was possible at one-g conditions (see Katz and Kocmond, 1973). The same experiment should be conducted with CCN of different substances, such as ammonium sulfate, which is currently regarded as one of the most abundant CCN materials. The obvious benefits of a fallout-free environment and the opportunity for acquiring significant scientific knowledge make these experiments of highest priority. Data generated from these tests will have immediate applications for cloud physicists and numerical modelers.

Testing of a water insoluble aerosol as CCN would be equally important since most natural nuclei are partly composed of some insoluble matter. Previously indicated difficulties with solvent removal in connection with particle generation could possibly be overcome by use of activated charcoal.

- Scavenging. Although a larger chamber would be preferable for scavenging studies, it is expected that diffusive losses in the thermal diffusion chamber would also be acceptable (according to Fuchs, 1964) if particle sizes are properly chosen. A tentative experiment could be carried out as follows: An aerosol with two distinctly different particle sizes can be introduced into the chamber and the supersaturation adjusted for activation of the larger particles only. After a certain time, the supersaturation can be increased so as to activate the smaller particles, too. By varying observation times and growth rates of the droplets grown on large CCN scavenging parameters can be deduced.

2. By slightly modifying the thermal diffusion chamber, it can be operated as a "haze chamber": If a salt solution instead of pure water is used on the chamber plates, conditions of slight subsaturation can also be achieved. This would make it possible to carry out the following experiment:

- CCN memory effect. In a procedure similar to the one of the proposed scavenging test, droplets formed on the more active particles of a two particle type aerosol can be allowed to interact with the non-activated particles. Subsequently, the droplets can be evaporated during a brief period of subsaturation. Reactivation of the more active particles will show the memory effect.

3. It is recommended that the previously mentioned experiment on coalescence proposed by Telford (1974) be considered for development into a carry-on package.

4. Experiments regarding CCN multiplication require that the humidity be decreased to very low subsaturation. This is not feasible within the diffusion chamber, and the removal of the sample from the chamber for drying makes it impossible to observe the same particle/droplet throughout the experiment. It is, therefore, recommended that this experiment be postponed until it can be carried out in an expansion chamber.

It is obviously impossible, in this initial effort, to develop a detailed experimental plan for the carry-on experiments listed above. It is recommended, however, that additional consideration be given to fully developing the ideas we have presented herein. In particular, the initial testing of the static thermal diffusion chamber will be an important first step toward the successful completion of the more complicated nucleation studies. The further development and testing of a haze chamber may also find special applications onboard the CPL. We feel that the experiments suggested here can be designed in such a manner as to provide pertinent immediate information for later application on the fully developed cloud physics laboratory.

3.6 REFERENCES

Fitzgerald, J.W., 1972: A Study of the Initial Phase of Cloud Droplet Growth by Condensation: Comparison Between Theory and Observation. Tech. Note No. 44, Cloud Physics Laboratory, Dept. Geophys. Sci., Univ. of Chicago, 144 pp.

Fuchs, N.A., 1964: The Mechanics of Aerosols. Pergamon Press. 408 pp.

Greco, E.V., L.R. Eaton, and H.C. Wilkinson, 1974: Zero-Gravity Atmospheric Cloud Physics Experiment Laboratory - Engineering Concepts/Design Tradeoffs, NASA CR-120500-120501.

Greco, E.V. and R.E. Turner, 1975: Cloud Physics Laboratory: A Step Toward Weather Control. Astronautics & Aeronautics, March 1975, 44-48.

Katz, U. and W.C. Kocmond, 1973: An Investigation of the Size-Supersaturation Relationship of Soluble Condensation Nuclei. J. Atmos. Sci., 30, 160-165.

Kocmond, W.C., E.J. Mack, U. Katz, and R.J. Pilié, 1972: Project FOG DROPS - Part II: Laboratory Investigation. NASA CR-2079.

Mack, E.J., U. Katz, C.W. Rogers, and R.J. Pilié, 1974: The Microstructure of California Coastal Stratus and Fogs at Sea, Project SEA FOG, Second Annual Summary Report, Calspan Report No. CJ-5404-M-1, Calspan Corp., Buffalo, N.Y. 14221.

Podzimek, J. and A.N. Saad, 1974: Metamorphosis of Sea Salt Particles at Changing Humidity. Abstr. 54th Annual AMS Conf., Honolulu, Jan. 8-11, 1974. Bull. AMS 54, 1106, 1973.

Ruskin, R.E. and W.C. Kocmond, 1971: Summary of Condensation Nucleus Investigations at the 1970 International Workshop on Condensation and Ice Nuclei. The Second International Workshop on Condensation and Ice Nuclei, Dept. Atmos. Sci., Colorado State University, 92-97.

Telford, J.W., 1974: Modeling of Cloud Draft Collisions with Low Gravity. Prepr. Conf. Cloud Phys., Tucson Arizona, October 21-24, 414-417.

Vaughan, O.H. and C.K. Hill, 1974: Drop Coalescence in Zero-Gravity Environment of Skylab IV. Bull. Amer. Meteor. Soc., 55, 1127-1130.

Wedding, J.B. and J.J. Stukel, 1974: Operational Limits of Vibrating Orifice Aerosol Generator. Env. Sci. Techn., 8, 456-457.

APPENDIX A

COMPUTER PROGRAM DOCUMENTATION FOR ADVECTION FOG MODEL

A.1 INTRODUCTION

The computer program used in the present study was basically the same one used previously and thoroughly documented in Mack et al. (1972). Since only minor changes were made in the computer program, the thorough documentation is not repeated. Documentation is presented here only for the few changes that were made in the computer program. However, for those readers who may want to run the program and who may not have access to the previous documentation, a description of the input variables and control indices is provided which is sufficient for the running of the program.

Changes from the previous program concern initialization of the two-dimensional model from upwind conditions generated by a one-dimensional model and computation of the turbulent exchange coefficients. The initialization utilizes the read-list capability of the model to which two new control indices have been added. The equations for computation of the turbulent exchange coefficient, which are described in the main text [Eqs. (6)-(15)] are fixed in the program and are not modified by input variables or control indices.

The program operates in cgs units with temperatures in degrees Kelvin. All input variables are in cgs units with the exception of the uniform spacing between columns (DELX) which is in meters. When liquid water content is read in from a list, the units used are grams of water per grams of air.

The program required 192K bytes of core storage for the execution step. The program was run on an IBM 370/168 operating under Release 1.6 VS. For one hour of meteorological time, eight horizontal grid columns with 43 vertical grid levels each, and a time step of two minutes, the execution took five seconds of machine time.

A.2 INITIALIZATION

Initialization of the wind, temperature, and moisture (vapor and liquid) occurs in a loop which is executed two times. The first time through all of the columns except the upwind column are initialized to contain identical values of the variables. The second time, variables are initialized for the upwind boundary (column one). The initialization procedure is controlled by input indices where values other than one provide for uniform or idealized profiles in the vertical. Index values of one provide for non-uniform profiles via the read-list input procedure.

When the variables are initialized by reading from a list, it is possible to initialize potential temperature, water vapor, and liquid water from any vertical grid level to the top of the model. This feature allows inversions to be specified in the initial profiles with an adiabatic temperature and uniform water vapor mixing ratio present below the inversion height. The grid level at which the non-uniform values begin are specified by KT for the potential temperature and by KR for both the water vapor and liquid water. In the two-dimensional mode of the model, when a list is provided for initialization, KT and KR are set equal to one.

In the read-list mode of initialization, the type of input is, of course, controlled by the format statement. In the program listing presented in Section A.4, a Z-format (hexadecimal) is used since the program is reading variables generated by the one-dimensional program.

A.3 SAMPLE SET OF INPUT CARDS

A. TIME VARIABLE CONSTANTS, TEMPERATURE AND WIND INPUT (card)

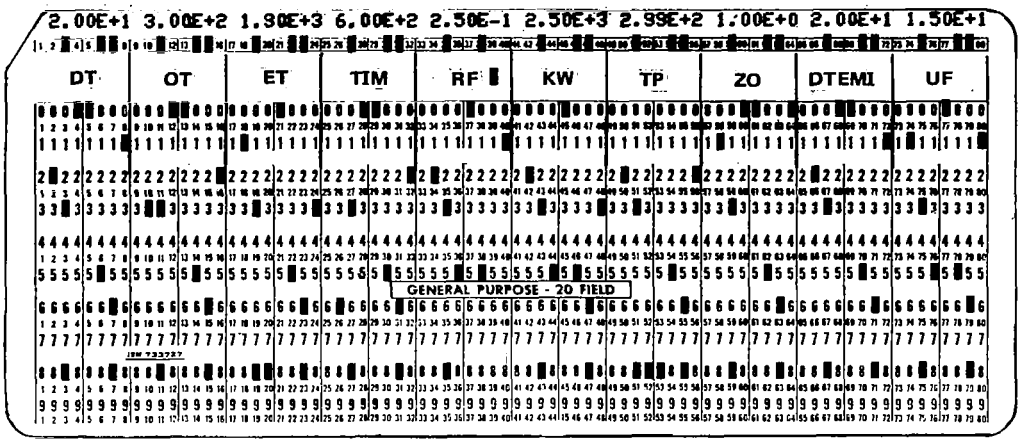

DT time step (seconds)

OT time interval at which output occurs (seconds)

ET length of simulation (seconds)

TIM time interval from t = 0 at which the colder or warmer surface temperature reaches its desired value (seconds)

RF fraction of surface black body radiation used as net upward infrared flux through upper boundary

KW a constant multiplied times liquid water content raised to the two-thirds power in equation (34) to obtain infrared absorption per cm

TP temperature in degrees Kelvin used to initialize the temperature profile to isothermal

ZO roughness length (cm)

DTEMI change from surface potential temperature in Column 1 needed to obtain a uniform surface temperature among the other columns when a uniform discontinuity in surface temperature is desired

UF friction velocity which enters into the quasi-adiabatic velocity profiles when they are used to initialize the velocity field (cm/sec)

B. CONTROL INDEX CARD (1 card)

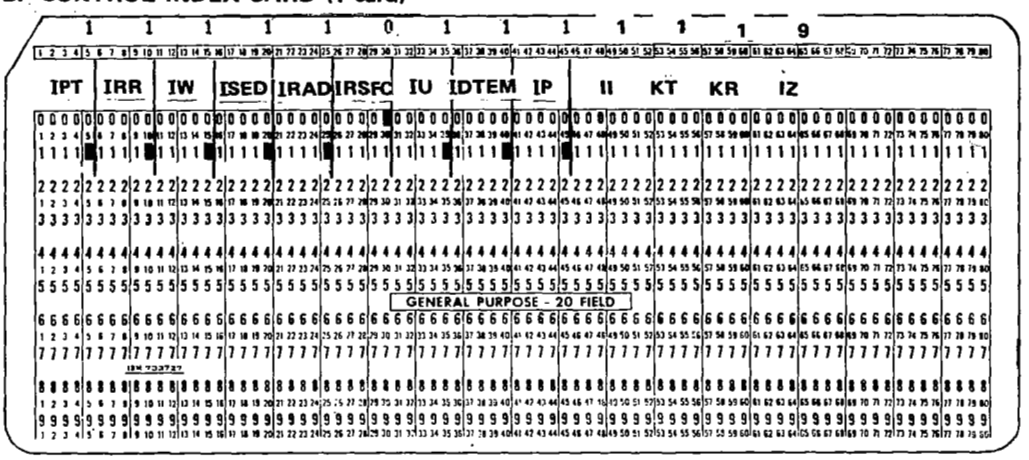

	= -1	PT(I,K) = $TP(\frac{1000}{P})^{K}$	, isothermal
IPT	= 0	PT(I,K) = PTI	, adiabatic
	= 1	PT(I,K) = LIST	
IRR	= 0	R(I,K) = RI	
	= 1	R(I,K) = LIST	
IW	= 0	W(I,K) = 0	
	= 1	W(I,K) = LIST	
ISED	= 1	sedimentation	
	≠ 1	no sedimentation	
IRAD	= 1	radiational cooling	
	≠ 1	no radiational cooling	

IF IRSFC = 0 R(I,1) = R(I,2)

= 1 R(I,1) = saturation mixing ratio at surface temperature and 1000 mb.

IU = 0 Quasi-adiabatic u and v profiles
= 1 u and v = LIST

IDTEM = 0 DTEM(I) = 0.0
= 1 DTEM(I) = DTEMI between ITEML and ITEMR, and equals zero elsewhere
= -1 DTEM(I) = LIST

HR = net radiative flux, cal cm^{-2} min^{-1} (positive upward)

COOL = rate of radiative cooling, ^{o}C hr^{-1}

IP = 0 No HR and COOL output provided

IP $\neq$ 0 HR and COOL output provided

II = 2 needed in velocity integration when turbulent exchange coefficient depends on local vertical gradient of velocity.

II = 1 when turbulent exchange coefficient does not depend on local conditions.

KT = vertical grid level to which first potential temperature in list is to be assigned.

KT = 1 when two-dimensional simulation is initialized from list generated by one-dimensional simulation.

KR performs same function for mixing ratio and liquid water content that KT does for the potential temperature.

IZ specifies number of the column for which wind, potential temperature, mixing ratio and liquid water will be punched out.

IZ = 2 in one-dimensional simulations.

C. GRID SPECIFICATION CARD (1 card)

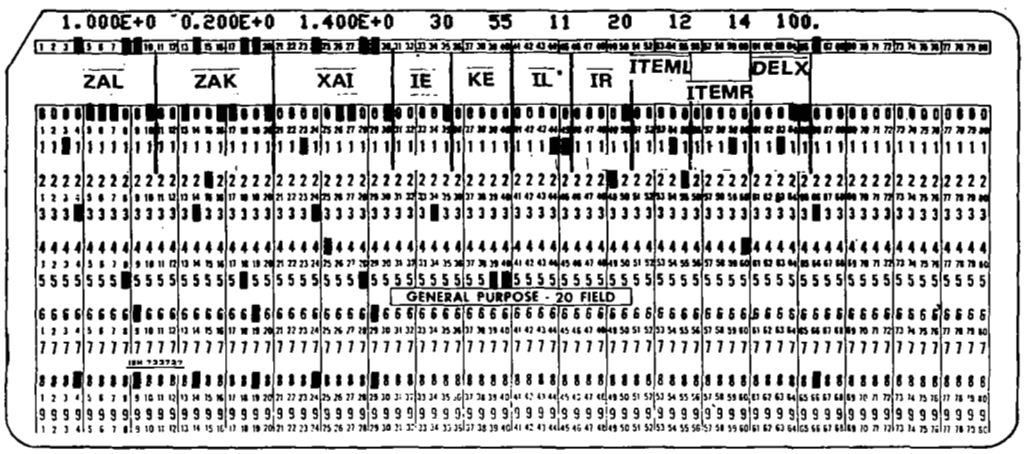

ZAL = height of lowest vertical grid point in the atmosphere (cm)

ZAK = expansion factor in the vertical

XAI = expansion factor in the horizontal

IE = number of horizontal columns

KE = number of vertical levels

IL = leftmost grid point of unexpanded grid

IR = rightmost grid point of unexpanded grid

ITEML = left and right I-limits on non-zero,

ITEMR uniform DTEM(I)

DELX = uniform X-spacing (meters)

D. OUTPUT FORMATS (2 cards)

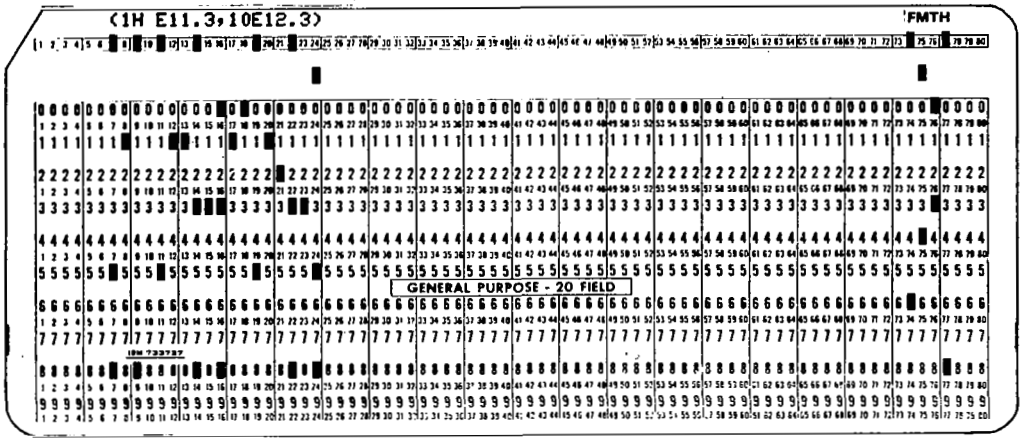

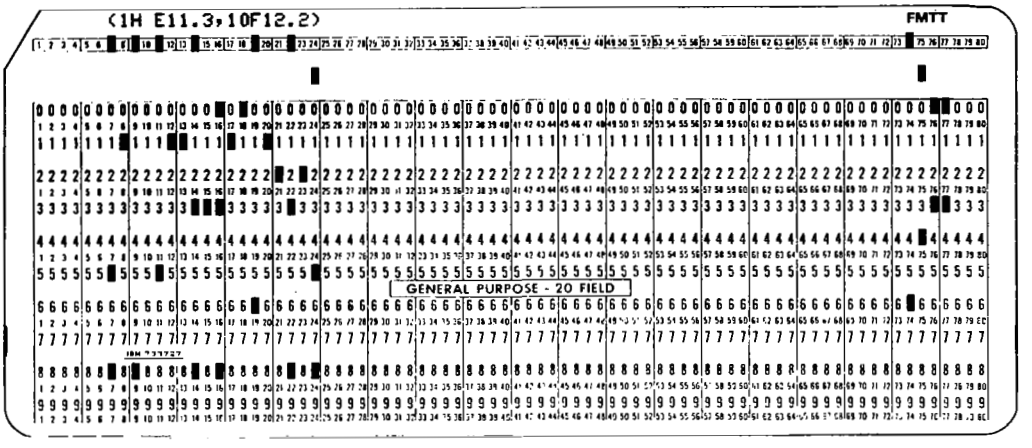

The printed output for the various quantities is in convenient standard units as shown in the format heading statements 3000-3800 in the program listing in Section A-4. In addition to previous outputs, the outputs of u and v component of the wind, the friction velocity and the eddy moisture flux have been added.

E. PROGNOSTIC VARIABLE INPUT, UNIFORM WITH HEIGHT (1 card)

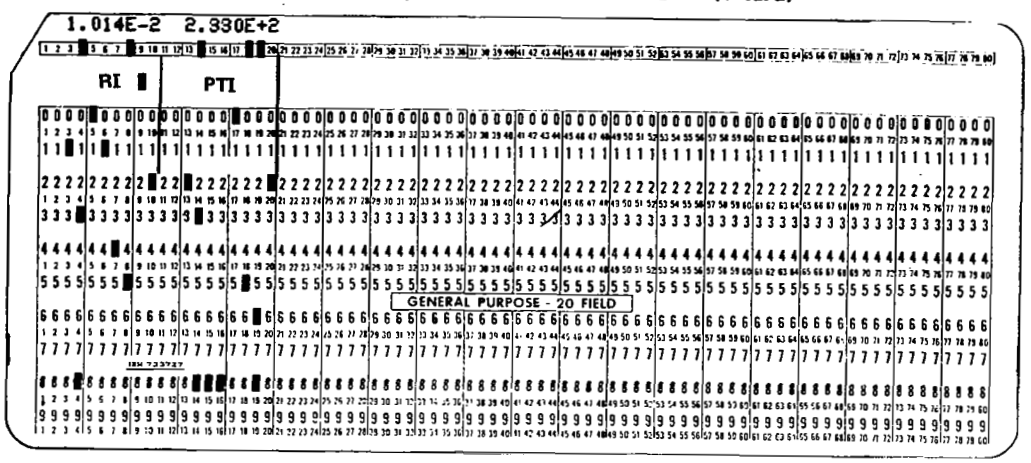

A.4 FORTRAN LISTING OF COMPUTER PROGRAM WITH COMMENT CARDS

```
C
C
C     TWO-DIMENSIONAL ADVECTION FOG MODEL
C     STEADY STATE MODEL
C
C     CALSPAN CORP. MARCH 1975 W.J. EADIE AND C.W.ROGERS
C
C
      REAL*8 PT,EPT,FPT,DPT,AT,CT,BT
      REAL*4 KA,INT,KW,L,LM,LMAX,KM
      COMMON PT(40,60),EPT(60),FPT(60),DPT,AT,CT,BT,
     8                 R(40,60),W(40,60),U(40,60),T(40,60),KA(40,60),
     7KM(40,60),
     1       INT(40,60),CPT(40,60),HC(40,60),X(40),DX(40),DTEM(40),
     2       P(60),ZA(60),DZA(60),                    ER(60),FR(60),EW(60),
     3       FW(60),EU(60),FU(60),Z(60),DZ(60),PR(60),L,DEN,CP,G,RA,RW,
     4       SIGMA,TIME,DT,TIM,UF,RF,KW,ZO,CV,UI,DTEMI,ZAK,XAI,DELX,CC,
     5       CH,CI,CK,CL,CR,CS,UU,FV(60),EV(60),V(40,60),     F,
     6       KE,KN,IE,IN,IL,IR,ISED,IRAD,IRSFC,IDTEM,ITEML,ITEMR,IP,II
      DIMENSION FMTH(11),FMTT(11)
C
C     PHYSICAL CONSTANTS
C
      L=592.
      DEN=1.23E-3
      CP=.240
      G=980.6
      RA=.0686
      RW=.1102
      SIGMA=1.355E-12
      CV=400.
      F=1.0E-4
      P(1)=1000.
C
C     DATA INPUT
C
   10 READ(5,1000,END=400) DT,OT,ET,TIM,RF,KW,TP,ZO,DTEMI,UF
      READ(5,1100) IPT,IRR,IW,ISED,IRAD,IRSFC,IU,IDTEM,IP,II,KT,KR,    1Z
      READ(5,1200) ZAL,ZAK,XAI,IE,KE,IL,IR,ITEML,ITEMR,DELX
      READ(5,1205) FMTH,FMTT
C
C     DATA LISTING
C
      WRITE(6,2000) DT,OT,ET,TIM,RF,KW,TP,ZO,DTEMI,UF
      WRITE(6,2100) IPT,IRR,IW,ISED,IRAD,IRSFC,IU,IDTEM,IP,II,KT,KR,    I
     1Z
      WRITE(6,2200) ZAL,ZAK,XAI,IE,KE,IL,IR,ITEML,ITEMR,DELX
C
C     WORKING CONSTANT DEFINITION
C
      CC=.622*(L**2)/(CP*RA)
      CR=KW*RF*SIGMA/(CP*DEN**.333)
      CI=KW*(DEN**.667)/2.
      CH=(L**2)/RW
      CK=.4*UF
      CS=G/4.186E+7
      IN=IE-1
      KN=KE-1
C
C     VERTICAL GRID SPECIFICATION
C
```

```
      ZA(1)=0.0
      ZA(2)=ZAL
      DZA(2)=ZAL
      DO 20 K=3,KE
      DZA(K)=(1.+ZAK)*DZA(K-1)
   20 ZA(K)=ZA(K-1)+DZA(K)
      DO 25 K=2,KE
      Z(K)=(ZA(K)+ZA(K-1))/2.
   25 CONTINUE
C
C     HORIZONTAL GRID SPECIFICATION
C
      DO 30 I=IL,IR
   30 X(I)=(I-IL)*DELX
      I1=IR+1
      DO 31 I=I1,IE
   31 X(I)=X(I-1)+XAI*(X(I-1)-X(I-2))
      IF(IL .EQ. 1) GO TO 33
      I1=IL-1
      DO 32 I2=1,I1
      I=I1-I2+1
   32 X(I)=X(I+1)-XAI*(X(I+2)-X(I+1))
   33 DO 35 I=2,IE
   35 DX(I)=X(I)-X(I-1)
C
C
C     VARIABLE INITIALIZATION
C
C
      READ(5,1300) RI,PTI
      WRITE(6,2300) RI,PTI
      TP=TP+.16
      PTI=PTI+.16
      W(1,1)=0.0
C
C     A-UNIFROM WITH HEIGHT
C
      DO 40 I=1,IE
      DO 40 K=1,KE
      W(I,K)=0.0
      R(I,K)=RI
       PT(I,K)=PTI
      IF(I .EQ. 1) P(K)=1000.*EXP(-G*ZA(K)/(4.186E+7*RA*TP))
C
C     B-ISOTHERMAL
C
      IF(IPT .EQ. -1) PT(I,K)=TP*((1000./P(K))**.286)
C
C     D-QUASI-ADIABATIC VELOCITY PROFILES
C
      IF(IU  .EQ. 0) U(I,K)=2.5*UF*ALOG((ZA(K)+ZO)/ZO)*COS(.1745)
      IF(IU  .EQ. 0) V(I,K)=2.5*UF*ALOG((ZA(K)+ZO)/ZO)*SIN(.1745)*(1-ZA(
     1K)/ZA(KE))
C
   40 CONTINUE
C
C     INITIALIZE 2-D SIMULATION  FROM 1-D SIMULATION
C     III=2 INITIALIZES UPWIND BOUNDARY  III=1 INITIALIZES REST OF DOMAIN
C
      DO 500 III=1,2
      IF(IU .EQ. 1) READ(5,4000) (U(1,K),K=1,KE)
```

```
      IF(IU .EQ. 1) READ(5,4000) (V(1,K),K=1,KE)
C
C      KT AND KR PERMIT NON-UNIFORM INITIALIZATION OF 1-DIMENSIONAL
C     SIMULATIONS FROM KT AND KR LEVELS TO TOP OF THE MODEL
C
      IF(IPT .EQ. 1) READ(5,5000) (PT(1,K),K=KT,KE)
      IF(IRR .EQ. 1) READ(5,4000) (R(1,K),K=KR,KE)
      IF(IW .EQ. 1) READ(5,4000) (W(1,K),K=KR,KE)
      IF(IU .EQ. 1) WRITE(6,2500) (U(1,K),K=1,KE)
      IF(IU .EQ. 1) WRITE(6,2500) (V(1,K),K=1,KE)
      IF(IPT .EQ. 1) WRITE(6,2400) (PT(1,K),K=1,KE)
      IF(IRR .EQ. 1) WRITE(6,2500) (R(1,K),K=KR,KE)
      IF(IW .EQ. 1) WRITE(6,2500) (W(1,K),K=1,KE)
C
      IF(IPT .EQ. 1) GO TO 45
      GO TO 60
C
C     PT AND W FROM VARIABLE LIST
C
   45 CONTINUE
C
C     INITIALIZE ONLY THE UPWIND COLUMN
C
      IF(III .EQ. 2) GO TO 501
C
C     INITIALIZATION ALL COLUMNS
C
      DO 50 I=2,IE
      DO 50 K=1,KE
      U(I,K)=U(1,K)
      V(I,K)=V(1,K)
      PT(I,K)=PT(1,K)
      R(I,K)=R(1,K)
   50 W(I,K)=W(1,K)
   60 CONTINUE
C
C     INITIALIZATION,EXCHANGE COEFFICIENT, INTEGRATED LIQUID WATER,AND
C     SPECIFIC HEAT OF MOIST AIR
C
  501 CONTINUE
      CL=14.*G*.16/PT(1,1)
      INT(1,1)=0.0
      T(1,1)=PT(1,1)
      DO 80 K=2,KE
      PR(K)=(1000./P(K))**.286
      DZ(K)=(1.+ZAK/2.)*(DZA(K)**2)
      T(1,K)=PT(1,K)/PR(K)
      DWZ=SQRT((U(1,K)-U(1,K-1))**2+(V(1,K)-V(1,K-1))**2)/DZA(K)
      IF(W(1,K) .GT. 0.0) GO TO 65
      CPT(1,K)=CP
C
C     INITIALIZATION OF EXCHANGE COEFFICIENTS COVERING NEUTRAL,STABLE AND
C     UNSTABLE CONDITIONS BETWEEN K=2 AND THE SURFACE
C
      S=(PT(1,K)-PT(1,K-1))/DZA(K)
      IF(K.EQ. 2) SS=S
      GO TO 70
   65 CPT(1,K)=CP+CH*RSF(T(1,K),P(K))/(T(1,K)**2)
      S=(T(1,K)-T(1,K-1))/DZA(K)+CS/CPT(1,K)
      IF(K .EQ. 2) SS=S
   70 IF(K .EQ. 2) GO TO 71
```

```
      IF(SS .GT. 0.) GO TO 75
      IF(SS .EQ. 0.) GO TO 77
      PHI=DSQRT(DSQRT(1.D0-15.D0*Z(K)/TL))
      KM(1,K)= .4*Z(K)*UF1*PHI
      KA(1,K)=KM(1,K)*PHI
      GO TO 79
   75 KM(1,K)=(.4*Z(K)*UF1)/(1.+5.*(Z(K)/TL))
      GO TO 78
   77 KM(1,K)=.4*Z(K)*UF1
   78 KA(1,K)=KM(1,K)
      GO TO 79
   71                 KM(1,2)=.16*SQRT(U(1,2)**2+V(1,2)**2)*DZA(2)/(ALOG(ZA
     1(2)/Z0)**2)
                      KA(1,2)=KM(1,2)
      UF1=SQRT(KM(1,2)*DWZ)
      IF(S .EQ. 0.0) GO TO 80
      TL=(UF1**3)*PT(1,2)/(.4*G*KA(1,2)*S)
       GO TO 80
C
C     SHIR-TYPE EXPONENTIAL DECREASE
C
   79  DEC=EXP(-8.*F*Z(K)/UF1)
      KM(1,K)=KM(1,K)*DEC
      KA(1,K)=KA(1,K)*DEC
   80 INT(1,K)=INT(1,K-1)+CI*(W(1,K)**.667+W(1,K-1)**.667)*DZA(K)
      CPT(1,1)=CPT(1,2)
      KA(1,1)=KA(1,2)
C
      IF(III .EQ. 2) GO TO 502
C     INITIALIZATION ALL COLUMNS
C
      DO 81 I=2,IE
      DO 81 K=1,KE
      IF(K .EQ. 1) W(I,K)=0.0
      T(I,K)=T(1,K)
      CPT(I,K)=CPT(1,K)
      KM(I,K)=KM(1,K)
      KA(I,K)=KA(1,K)
   81 INT(I,K)=INT(1,K)
  500 CONTINUE
  502 CONTINUE
C
C     INITIALIZATION OF SURFACE TEMPERATURE DIFFERENCE
C
      IF(IDTEM .EQ. -1) GO TO 86
      DO 85 I=1,IN
      IF(IDTEM .EQ. 0) DTEM(I)=0.0
      IF(IDTEM .EQ. 1) DTEM(I)=DTEMI
      IF((IDTEM .EQ. 1) .AND. (I .LT. ITEML)) DTEM(I)=0.0
      IF((IDTEM .EQ. 1) .AND. (I .GT. ITEMR)) DTEM(I)=0.0
   85 CONTINUE
      GO TO 87
   86 READ(5,1400) (DTEM(I),I=2,IN)
      WRITE(6,2400) (DTEM(I),I=2,IN)
      DTEM(1)=0.0
      DTEM(IE)=0.0
C
C     UPPER BOUNDARY CONDITION FOR IMPLICIT INTEGRATION
C
   87 EU(KE)=0.
      EV(KE)=0.
```

```
      EPT(KE)=0.0
      ER(KE)=0.0
      EW(KE)=0.0
      FU(KE)=U(1,KE)
      FV(KE)=V(1,KE)
      FPT(KE)=PT(1,KE)
      FR(KE)=R(1,KE)
      FW(KE)=W(1,KE)
C
C     OUTPUT TIME ,END TIME, AND TIME STEP CONTROL
C
      TIME=0.0
      PRT=DT
   90 IF(TIME .LT. PRT) GO TO 95
      PRT=TIME+DT
      GO TO 200
   95 IF(TIME .GE. ET) GO TO 10
      TIME=TIME+DT
      CALL STEP
      GO TO 90
  200 CONTINUE
C
C
C     OUTPUT
C
C
C
C     EDDY HEAT FLUX OUTPUT
C
  300 WRITE(6,3000)
      DO 311 I=1,IE
      DO 310 K=3,KN
      IF(CPT(I,K) .LE. CP) HC(I,K)=-DEN*CP*((KA(I,K+1)*(PT(I,K+1)-PT(I,K
     1))/(ZA(K+1)-ZA(K)))+(KA(I,K)*(PT(I,K)-PT(I,K-1))/(ZA(K)-ZA(K-1)))
     2*2.1
  310 IF(CPT(I,K) .GT. CP) HC(I,K)=-DEN*CPT(I,K)*(((KA(I,K)+KA(I,K+1))/2
     1.)*((T(I,K+1)-T(I,K-1))/(ZA(K+1)-ZA(K-1))+GS/CPT(I,K)))*4.2
      WINDV2=SQRT(U(I,2)**2+V(I,2)**2)*.07
      IF(CPT(I,2) .LE. CP) HC(I,2)=-DEN*CP*60.*.16*WINDV2*(PT(I,2)-PT(I,
     11))/(ALOG(ZA(2)/ZO)**2)
      IF(CPT(I,2) .GT. CP) HC(I,2)=-DEN*CPT(I,2)*60.*.16*WINDV2*(T(I,2)-
     1T(I,1)+GS*ZA(2)/CPT(I,2))/(ALOG(ZA(2)/ZO)**2)
      HC(I,1)=HC(I,2)
      HC(I,KE)=HC(I,KN)
  311 CONTINUE
      CALL PRNT(HC,FMTH)
C
C     LOCAL FRICTION VELOCITY OUTPUT
C
      WRITE(6,3008)
      DO 313 I=1,IE
      DO 312 K=3,KN
      FLUX=(KM(I,K+1)*SQRT((U(I,K+1)-U(I,K))**2+(V(I,K+1)-V(I,K))**2)/DZ
     1A(K+1) +KM(I,K)*SQRT((U(I,K)-U(I,K-1))**2+(V(I,K)-V(I,K-1))**2)/DZ
     2A(K))/2.
      IF(FLUX .GT. 0.) HC(I,K)=SQRT(FLUX)
  312 CONTINUE
      WINDV2=SQRT(U(I,2)**2+V(I,2)**2)
      HC(I,2)=.4*WINDV2/ALOG(ZA(2)/ZO)
      HC(I,1)=HC(I,2)
  313 HC(I,KE)=HC(I,KN)
```

```
      CALL PRNT(HC,FMTH)
C
C
C     PRINT AND PUNCH OF PROGNOSTIC VARIABLES FOR INPUT AS UPWIND CONDITIONS
C
C
C     WIND OUTPUT
C
      WRITE(6,3009)
      DO 314 I=1,IE
      DO 314 K=1,KE
  314 HC(I,K)=1.0E-2*U(I,K)
      CALL PRNT(HC,FMTH)
      WRITE(6,3010)
      DO 316 I=1,IE
      DO 316 K=1,KE
  316 HC(I,K)=1.0E-2*V(I,K)
      CALL PRNT(HC,FMTH)
      WRITE(7,4000) (U(IZ,K),K=1,KE)
      WRITE(7,4000) (V(IZ,K),K=1,KE)
C
C     TEMPERATURE OUTPUT
C
      WRITE(6,3100)
      CALL PRNT(T,FMTT)
      WRITE(7,5000) (PT(IZ,K),K=1,KE)
C
C     MIXING RATIO OUTPUT
C
      WRITE(6,3200)
      CALL PRNT(R,FMTH)
      WRITE(7,4000) (R(IZ,K),K=1,KE)
C
C     LIQUID WATER CONTENT OUTPUT
C
      WRITE(6,3300)
      DO 315 I=1,IE
      DO 315 K=1,KE
  315 HC(I,K)=DEN*W(I,K)*1.0E+6
      CALL PRNT(HC,FMTH)
      WRITE(7,4000) (W(IZ,K),K=1,KE)
C
C     DEW POINT DEPRESSION OUTPUT
C
      WRITE(6,3400)
      DO 320 I=1,IE
      DO 320 K=1,KE
C
C     DEW POINT DEPRESSION COMPUTATION
C
      E=P(K)*R(I,K)/(.62465+R(I,K))
      T1=T(I,K)
      DO 318 M=1,3
      RS=RSF(T1,P(K))
      ES=P(K)*RS/(.62465+RS)
      EE=E/ES
  318 T1=T1+(T1-35.86)*ALOG(EE)/17.26939
  320 HC(I,K)=T(I,K)-T1
      CALL PRNT(HC,FMTH)
C
C     TURBULENT EXCHANGE COEFFICIENT OUTPUT
```

```
C
      WRITE(6,3500)
      DO 331 I=1,IE
      DO 330 K=3,KN
      EX=(KA(I,K)+KA(I,K+1))/2.
  330 HC(I,K)=EX
      HC(I,2)=.16*SQRT(U(I,2)**2+V(I,2)**2)*ZA(2)/ALOG(ZA(2)/ZO)
      HC(I,1)=0.
  331 HC(I,KE)=HC(I,KN)
      CALL PRNT(HC,FMTH)
C
      IF(IP .EQ. 0) GO TO 95
C
C     RADIATIVE FLUX OUTPUT
C
      WRITE(6,3600)
      DO 340 I=1,IE
      DO 340 K=1,KE
      HR=RF*SIGMA*(T(I,1)**4)*EXP(-INT(I,KE)+INT(I,K))*60.
  340 HC(I,K)=HR
      CALL PRNT(HC,FMTH)
C
C     RADIATIVE COOLING RATE OUTPUT
C
      WRITE(6,3700)
      DO 350 I=1,IE
      DO 350 K=1,KE
      COOL=-3600.*(W(I,K)**.667)*CR*(T(I,1)**4.)*EXP(-INT(I,KE)+INT(I,K)
     1)*CP/CPT(I,K)
  350 HC(I,K)=COOL
      CALL PRNT(HC,FMTH)
C
C     WATER VAPOR FLUX OUTPUT
C
      WRITE(6,3800)
      DO 361 I=1,IE
      DO 360 K=3,KN
      HC(I,K)=-DEN*.5*((KA(I,K+1)*(R(I,K+1)-R(I,K))/(ZA(K+1)-ZA(K)))+(KA
     1(I,K)*(R(I,K)-R(I,K-1))/(ZA(K)-ZA(K-1))))
  360 CONTINUE
      WINDV2=SQRT(U(I,2)**2+V(I,2)**2)
      HC(I,2)=-DEN*.16*WINDV2*(R(I,2)-R(I,1))/(ALOG(ZA(2)/ZO)**2)
      HC(I,1)=HC(I,2)
       HC(I,KE)=HC(I,KN)
  361  CONTINUE
      CALL PRNT(HC,FMTH)
      GO TO 95
  400 STOP
 1000 FORMAT(10E8.2)
 1100 FORMAT(14I5)
 1200 FORMAT(3E10.3,6I5,-2PF6.0)
 1205 FORMAT(11A4/11A4)
 1300 FORMAT(4E10.3)
 1400 FORMAT(8F10.2)
 1500 FORMAT(8E10.3)
 2000 FORMAT(1H1,////,60X,10HINPUT DATA,//,1H0,1P10E10.3)
 2100 FORMAT(1H0,14I5)
 2200 FORMAT(1H0,1P3E10.3,0P6I5,-2PF6.0)
 2300 FORMAT(1H0,4E10.3)
 2400 FORMAT(1H0,8F10.2)
 2500 FORMAT(1H0,8E10.3)
```

```
 3000 FORMAT(30H1EDDY HEAT FLUX IN WATTS/CM**2///)
 3008 FORMAT(28H1FRICTION VELOCITY IN CM/SEC///)
 3009 FORMAT(29H1U COMPONENT OF WIND IN M/SEC///)
 3010 FORMAT(29H1V COMPONENT OF WIND IN M/SEC///)
 3100 FORMAT(21H1TEMPERATURE IN DEG K///)
 3200 FORMAT(20H1MIXING RATIO IN G/G///)
 3300 FORMAT(31H1LIQUID WATER CONTENT IN G/M**3///)
 3400 FORMAT(30H1DEW POINT DEPRESSION IN DEG C///)
 3500 FORMAT(44H1TURBULENT EXCHANGE COEFFICIENT IN CM**2/SEC///)
 3600 FORMAT(31H1RADIATIVE FLUX IN CAL/CM**2MIN///)
 3700 FORMAT(30H1RADIATIVE COOLING IN DEG C/HR///)
 3800 FORMAT(34H1EDDY MOISTURE FLUX IN G/CM**2 SEC///)
C
C      Z-FORMAT EQUALS HEXADECIMAL FORMAT
C
 4000 FORMAT(10Z8)
 5000 FORMAT(5Z16)
      END
C
C      INTEGRATION SUBROUTINE
C
C      INTEGRATE ONE TIME STEP AND COMPUTE NEW PROGNOSTIC & DIAGNOSTIC
C      VARIABLES
C
      SUBROUTINE STEP
       REAL*8 PT,EPT,FPT,DPT,AT,CT,BT
      REAL*4 KA,INT,KW,L,LM,LMAX,KM
      COMMON PT(40,60),EPT(60),FPT(60),DPT,AT,CT,BT,
     8                  R(40,60),W(40,60),U(40,60),T(40,60),KA(40,60),
     7KM(40,60),
     1        INT(40,60),CPT(40,60),HC(40,60),X(40),DX(40),DTEM(40),
     2        P(60),ZA(60),DZA(60),                    ER(60),FR(60),EW(60),
     3        FW(60),EU(60),FU(60),Z(60),DZ(60),PR(60),L,DEN,CP,G,RA,RW,
     4        SIGMA,TIME,DT,TIM,UF,RF,KW,ZO,CV,UI,DTEMI,ZAK,XAI,DELX,CC,
     5        CH,CI,CK,CL,CR,CS,UU,FV(60),EV(60),V(40,60),      F,
     6        KE,KN,IE,IN,IL,IR,ISED,IRAD,IRSFC,IDTEM,ITEML,ITEMR,IP,II
C
C      UPWIND DO LOOP OVER HORIZONTAL GRID SYSTEM
C
      DO 80 M=2,IN
      I=IN+2-M
C
C      DOWNWARD DO LOOP OVER VERTICAL GRID SYSTEM TO SET UP IMPLICIT
C      INTEGRATION
C
      DO 20 N=2,KN
      K=KN+2-N
      DD=DT/DZ(K)
      A=DD*KA(I,K+1)/(1.+ZAK)
      AW=A
      AU=DD*KM(I,K+1)/(1.+ZAK)
      AUU=II*AU
      AT=A
      C=DD*KA(I,K)
      CW=C
      CU=DD*KM(I,K)
      CUU=II*CU
      CT=C
      IF(ISED .NE.1) GO TO 10
C
C      DROP SEDIMENTATION
```

```
C
      DS=CV*DD*DZA(K)/2.
      AW=AW+DS*(W(I,K+1)**.667)
      CW=CW-DS*(W(I,K-1)**.667)
C
   10 B=1.+A+C
      BUU=1.+AUU+CUU
      BT=1.+AT+CT
      DPT=PT(I,K)-U(I,K)*(PT(I,K)-PT(I-1,K))*DT/DX(I)
C
C     RADIATIONAL COOLING
C
      IF((IRAD .EQ. 1) .AND. (W(I,K) .GT. 0.0)) DPT=DPT-CR*W(I,K)*(PT(I,
     11)**4.)*EXP(-INT(I,KE)+INT(I,K))*PR(K)*DT/(W(I,K)**.333)
C
       DU=U(I,K)*(1.+(II-1)*(AU+CU))-(II-1)*(AU*U(I,K+1)+CU*U(I,K-1))
     1-U(I,K)*(U(I,K)-U(I-1,K))*DT/DX(I) + F*(V(I,K)-V(I,KE))*DT
       DV=V(I,K)*(1.+(II-1)*(AU+CU))-(II-1)*(AU*V(I,K+1)+CU*V(I,K-1))
     1-U(I,K)*(V(I,K)-V(I-1,K ))*DT/DX(I) + F*(U(I,KE)-U(I,K))*DT
      DW = W(I,K)-U(I,K)*( W(I,K)- W(I-1,K))*DT/DX(I)
      DR = R(I,K)-U(I,K)*( R(I,K)- R(I-1,K))*DT/DX(I)
      EU(K)=CUU/(BUU-AUU*EU(K+1))
      EV(K)=CUU/(BUU-AUU*EV(K+1))
      EPT(K)=CT/(BT-AT*EPT(K+1))
      ER(K)=C/(B-A*ER(K+1))
      EW(K)=CW/(B-AW*EW(K+1))
      FU(K)=(DU+AUU*FU(K+1))*EU(K)/CUU
      FV(K)=(DV+AUU*FV(K+1))*EV(K)/CUU
      FPT(K)=(DPT+AT*FPT(K+1))*EPT(K)/CT
      FR(K)=(DR+A*FR(K+1))*ER(K)/C
      FW(K)=(DW+AW*FW(K+1))*EW(K)/CW
   20 CONTINUE
C
C     UPDATE SURFACE BOUNDARY CONDITION
C
      IF(TIME .LE. TIM) PT(I,1)=PT(1,1)+DTEM(I)*TIME/TIM
      IF(TIME .LE. TIM) T(I,1)=PT(I,1)
      IF(IRSFC .EQ. 0) R(I,1)=FR(2)/(1.-ER(2))
C
C     SATURATION SURFACE BOUNDARY CONDITION ON R
C
      IF(IRSFC  .EQ. 1) R(I,1)=RSF(T(I,1),1000.)
C
C     UPWARD DO LOOP OVER VERTICAL GRID SYSTEM TO COMPUTE NEW PROGNOSTIC
C     AND DIAGNOSTIC VARIABLES
C
      INT(I,1)=0.0
      DO 70 K=2,KE
      IF(K .EQ. KE) GO TO 40
      U(I,K)=EU(K)*U(I,K-1)+FU(K)
      V(I,K)=EV(K)*V(I,K-1)+FV(K)
      PT(I,K)=EPT(K)*PT(I,K-1)+FPT(K)
      R(I,K)=ER(K)*R(I,K-1)+FR(K)
      W(I,K)=EW(K)*W(I,K-1)+FW(K)
C
C     COMPUTE TEMPERATURE
C
      T(I,K)=PT(I,K)/PR(K)
C
C     SATURATION ADJUSTMENT
C
```

```
      RS=RSF(T(I,K),P(K))
      IF((R(I,K) .LE. RS) .AND. (W(I,K) .LE. 0.0)) GO TO 40
      DR=(R(I,K)-RS)/(1.+CC*RS/(T(I,K)**2))
      IF(R(I,K) .GT. RS) GO TO 30
      IF(-DR .LE. W(I,K)) GO TO 30
      DR=-W(I,K)
   30 T(I,K)=T(I,K)+DR*L/CP
      PT(I,K)=T(I,K)*PR(K)
      R(I,K)=R(I,K)-DR
      W(I,K)=W(I,K)+DR
C
C     COMPUTE NEW VALUES OF INT, CPT, AND KA
C
   40 IF(W(I,K) .LT. 0.0) W(I,K)=0.0
      INT(I,K)=INT(I,K-1)+CI*(W(I,K)**.667+W(I,K-1)**.667)*DZA(K)
      DWZ=SQRT((U(I,K)-U(I,K-1))**2+(V(I,K)-V(I,K-1))**2)/DZA(K)
      IF(W(I,K) .GT. 0.0) GO TO 50
      CPT(I,K)=CP
C
C     DIAGNOSIS OF EXCHANGE COEFFICIENTS COVERING NEUTRAL,STABLE AND
C     UNSTABLE CONDITIONS BETWEEN K=2 AND THE SURFACE
C
      S=(PT(I,K)-PT(I,K-1))/DZA(K)
      IF(K.EQ. 2) SS=S
      GO TO 60
   50 CPT(I,K)=CP+CH*RSF(T(I,K),P(K))/(T(I,K)**2)
      S=(T(I,K)-T(I,K-1))/DZA(K)+CS/CPT(I,K)
      IF(K .EQ. 2) SS=S
   60 IF(K .EQ. 2) GO TO 71
      IF(SS .GT. 0.) GO TO 75
      IF(SS .EQ. 0.) GO TO 77
      PHI=DSQRT(DSQRT(1.D0-15.D0*Z(K)/TL))
      KM(I,K)= .4*Z(K)*UF1*PHI
      KA(I,K)=KM(I,K)*PHI
      GO TO 79
   75 KM(I,K)=(.4*Z(K)*UF1)/(1.+5.*(Z(K)/TL))
      GO TO 78
   77 KM(I,K)=.4*Z(K)*UF1
   78 KA(I,K)=KM(I,K)
      GO TO 79
   71              KM(I,2)=.16*SQRT(U(I,2)**2+V(I,2)**2)*DZA(2)/(ALOG(ZA
     1(2)/ZO)**2)
                  KA(I,2)=KM(I,2)
      UF1=SQRT(KM(I,2)*DWZ)
      IF(S .EQ. 0.0) GO TO 70
      TL=(UF1**3)*PT(I,2)/(.4*G*KA(I,2)*S)
      GO TO 70
C
C     SHIR-TYPE EXPONENTIAL DECREASE
C
   79  DEC=EXP(-8.*F*Z(K)/UF1)
      KM(I,K)=KM(I,K)*DEC
      KA(I,K)=KA(I,K)*DEC
C
   70 CONTINUE
C
C     UPDATE SURFACE BOUNDARY CONDITION ON R AFTER SATURATION ADJUSTMENT
C     IF NO FLUX CONDITION USED
C
      IF(IRSFC .EQ. 0) R(I,1)=R(I,2)
C
```

```
   80 CONTINUE
C
C     UPDATE DOWNWIND BOUNDARY CONDITION
C
      DO 90 K=1,KE
      PT(IE,K)=PT(IN,K)
      U(IE,K)=U(IN,K)
      V(IE,K)=V(IN,K)
      R(IE,K)=R(IN,K)
      W(IE,K)=W(IN,K)
      KA(IE,K)=KA(IN,K)
      KM(IE,K)=KM(IN,K)
      T(IE,K)=T(IN,K)
      CPT(IE,K)=CPT(IN,K)
      INT(IE,K)=INT(IN,K)
   90 CONTINUE
      RETURN
      END
C
C
C
C     PRINT SUBROUTINE
C
      SUBROUTINE PRNT(O,FORM)
      REAL*8 PT,EPT,FPT,DPT,AT,CT,BT
      REAL*4 KA,INT,KW,L,LM,LMAX,KM
      COMMON PT(40,60),EPT(60),FPT(60),DPT,AT,CT,BT,
     8                 R(40,60),W(40,60),U(40,60),T(40,60),KA(40,60),
     7KM(40,60),
     1       INT(40,60),CPT(40,60),HC(40,60),X(40),DX(40),DTEM(40),
     2       P(60),ZA(60),DZA(60),                ER(60),FR(60),EW(60),
     3       FW(60),EU(60),FU(60),Z(60),DZ(60),PR(60),L,DEN,CP,G,RA,RW,
     4       SIGMA,TIME,DT,TIM,UF,RF,KW,ZO,CV,UI,DTEMI,ZAK,XAI,DELX,CC,
     5       CH,CI,CK,CL,CR,CS,UU,FV(60),EV(60),V(40,60),     F,
     6       KE,KN,IE,IN,IL,IR,ISED,IRAD,IRSFC,IDTEM,ITEML,ITEMR,IP,II
      DIMENSION O(40,60),FORM(11)
C
C     OUTPUT DOCUMENTATION
C
      WRITE(6,4000) TIME,DTEMI,ITEML,ITEMR
C
C     PAGE 1 COLUMNS 1-10
C
      WRITE(6,4100) (X(I),I=1,10)
      DO 450 J=1,KE
      K=KE-J+1
  450 WRITE(6,FORM) ZA(K),(O(I,K),I=1,10)
C
      IF(IE .LT. 11) GO TO 490
C
C     PAGE 2 COLUMNS 11-20
C
      WRITE(6,4105) (X(I),I=11,20)
      DO 460 J=1,KE
      K=KE-J+1
  460 WRITE(6,FORM) ZA(K),(O(I,K),I=11,20)
C
      IF(IE .LT. 21) GO TO 490
C
C     PAGE 3 COLUMNS 21-30
C
```

```
      WRITE(6,4105) (X(I),I=21,30)
      DO 470 J=1,KE
      K=KE-J+1
  470 WRITE(6,FORM) ZA(K),(O(I,K),I=21,30)
C
      IF(IE .LT. 31) GO TO 490
C
C     PAGE 4 COLUMNS 31-IE
C
      WRITE(6,4105) (X(I),I=31,IE)
      DO 480 J=1,KE
      K=KE-J+1
  480 WRITE(6,FORM) ZA(K),(O(I,K),I=31,IE)
C
  490 CONTINUE
 4000 FORMAT(6HOTIME=,F7.0,4H SEC,6X,6HDTEMI=,F5.1,2H K,6X,6HITEML=,I2,2
     1X,6HITEMR=,I2)
 4100 FORMAT(1HO,6HX(KM)=,6X,10(-5PF12.2) / 1H ,3X,5HZ(CM))
 4105 FORMAT(1H1,6HX(KM)=,6X,10(-5PF12.2) / 1H ,3X,5HZ(CM))
      RETURN
      END
C
C
C     SATURATION MIXING RATIO AS A FUNCTION OF TEMPERATURE A AND
C     PRESSURE B
C
      FUNCTION RSF(A,B)
      ES=6.1078*EXP(17.26939*(A-273.16)/(A-35.86))
      RSF=.62465*ES/(B-ES)
      RETURN
      END
C
C
                      DATA CARDS
 1.20E+2 1.80E+3 3.60E+3 1.80E+3 2.50E-1  .71E+1 2.87E+2 1.00E-2 0.00E+0 5.00E+0
    1     1     1     1     1     1     1     1     1     1     1     1   43    9
  1.000E+1  0.200E+0  2.000E+0   10    43    1     6     2     9 1000.
      (1H 1PE11.2,10E12.2)                                                  FMTH
      (1H 1PE11.2,0P10F12.2)                                                FMTT
  1.090E-2  2.870E+2
C
      PROGNOSTIC VARIABLE(U,V,PT,R AND W) INPUT IF USED
C
```

A.5 REFERENCES

Mack, E.J., W.J. Eadie, C.W. Rogers, W.C. Kocmond, and R.J. Pilié, 1972: A Field Investigation and Numerical Simulation of Coastal Fog, Calspan Report No. CJ-5055-M-1, Calspan Corporation, Buffalo, N.Y. 14221.